Modeling of fission product release during severe accidents with the fuel performance code ALCYONE

A. Germain, J. Sercombe, C. Riglet-Martial, C. Introïni, L. Noirot, Y. Pontillon, Ph. Maugis

Modeling of Fission Product release during Severe Accidents with the fuel performance code ALCYONE

A. Germain[a], J. Sercombe[a], C. Riglet-Martial[a], C. Introïni[a], L. Noirot[a], Y. Pontillon[a], Ph. Maugis[b]

[a] CEA, DES, IRESNE, DEC, 13018 Saint-Paul-Lez-Durance, France
[b] Aix-Marseille University, CNRS, IM2NP, 13397 Marseille, France

April 9, 2021

Abstract

This paper presents simulations of four tests performed on medium to high burnup fuel during the VERCORS and VERDON experimental programs. The tests are representative of a Severe Accident (SA) sequence with a temperature increase up to fuel-clad melting and oxidizing/reducing conditions within the furnace. The simulations are performed with the fuel performance code ALCYONE where irradiated fuel thermochemistry and fission gas release are coupled. In this paper, the impact of the radial burnup and Fission Product (FP) profiles within the fuel pellet on the FP release from the sample during the SA sequence is studied. Simulations of the fuel sample behavior during nominal irradiation in commercial reactors are first performed to assess the initial state of the fuel. The simulations of the SA sequences include a burnup dependent fission gas release model. The simulated release curves of various volatile and semi-volatile FPs (Xe, I, Te, Cs, Mo and Ba) are compared successfully to on-line measurements. The impact of the burnup and FP radial profiles on both the thermochemical equilibria within the pellet and the FP release kinetics is discussed. It is shown that the FP release from the fuel pellets is not significantly increased by the consideration of the burnup and FP radial profiles. This conclusion is due to the limited radial extension of the peaked burnup radial profile in the fuel pellet and to the uniform temperature of the fuel samples.

1 Introduction

During a Severe Accident (SA), Fission Product (FP) release can occur with potential environmental consequences. It is therefore of primary importance to well understand the phenomena behind FP release. Experimental programs have been launched worldwide to study and quantify FP release during SAs. Among them, separate-effect tests were performed at the CEA in 2 different programs: VERCORS [1][2][3][4] and VERDON [5][6][7]. These tests were launched to study the impact of several parameters on FP release: burnup of the fuel, geometry of the fuel fragments, oxidizing/reducing atmosphere, etc... The comparison of FP release kinetics during annealing tests with close temperature and atmospheric conditions but performed on medium ($\sim$38 GWd/tU) and high burnup fuel samples ($\sim$72 GWd/tU) showed the acceleration with burnup of the FP release kinetics and magnitude.

A recent review on thermodynamically informed codes pointed out the lack of advanced thermochemical calculations in SA codes compared to fuel performance codes [8]. Advanced thermochemical calculations rely on extensive Thermodynamic DataBases (TDB) and on the use of a Gibbs Energy Minimization (GEM) solver to determine the most probable phases and chemical species at given temperature and pressure conditions from the complex system at hand in irradiated fuels. In the last two years, several research teams have made progress on this aspect. Piro [9] calculated fission gas speciation, fuel volatilization, changes in the fuel stoichiometry, fuel melting and fission product solubility in irradiated CANDU fuel under representative SA conditions with the ThermoCalc commercial software and the TAF-ID [10] (Thermodynamics for Advanced Fuels International Database). The calculations were used to replace previous thermodynamic look-up tables used by the SOURCE code [11] which includes time-dependent phenomena related to FP diffusion. A coupling between the SA code MELCOR [12] where FP diffusion is handled and thermodynamic calculations with the GEMS code [13] and the HERACLES TDB [14] has been proposed by Nichenko et al. [15]. Applied to the VERDON 1 test, the calculated speciation of Mo and Ba in the solid, liquid and gas phases led to a significant improvement of the modeling of the release of these semi-volatile FPs. A coupling between a fission gas transport equation and thermodynamic calculations performed with the solver OPENCALPHAD and two TDBs, the TBASE developed at CEA, France and the TAF-ID, has been proposed by Germain et al. [16][17]. Fission gas speciation, fuel volatilization, changes in fuel stoichiometry, FP solubility, fuel-clad melting and FP/actinide release during the VERCORS 4/5, RT6 and VERDON 1 tests have been successfully reproduced in this work, showing again the potential benefits of advanced thermodynamic calculations in SA simulations.

The second aspect that is generally lacking in SA codes compared to fuel performance codes is the precise description of the irradiated fuel state before the SA scenario. SA codes generally consider the fuel pellet as a single entity characterized by an average burnup and FP content [12] [18]. While this hypothesis is convenient to reduce the computational time, it is far from the fuel state after irradiation in a commercial Pressurized Water Reactor (PWR). Due to the build-up of Pu at the fuel pellet rim, the fission rate increases at the pellet periphery leading to much higher quantities of FPs and burnup in this region as irradiation proceeds. The development of the High Burnup Structure (HBS) at the pellet rim with a specific microstructure [19][20] (e.g., porosity, grain size) and hence an increased potential for FP release is one of the consequences of this non uniform irradiation. The strong radial temperature gradient at hold during nominal irradiation is another reason for the pronounced inhomogeneity of the fuel samples prior to a SA. These aspects are generally taken into account in more or less details in fuel performance codes [21]. In view of the pronounced impact of the average burnup of the fuel on the FP release kinetics, as showed by the VERCORS/VERDON tests [5], it is therefore of importance to evaluate the impact of the radial burnup and FP gradients in the fuel pellet on the total FP release. In recent years, some tentative coupling between the fuel performance code TRANSURANUS [22] and the thermochemical - gas diffusion code MFPR [23] have been presented in this aim but no clear conclusions were reported [24].

In this paper, the coupling between thermochemical equilibrium calculations and fission gas release already implemented in the fuel performance code ALCYONE [25][26][27] for Pellet Cladding Interaction (PCI) analyses is extended to SAs to study the impact of radial burnup and FP gradients on FP release. Following the approach proposed by Germain et al. [16], a burnup dependent Fission Gas Release (FGR) model describing

the transport and release of all the gases formed in the fuel pellet (the noble gases and the gases formed from chemically reactive FPs) is developed. The coupling of this model with the OPENCALPHAD solver and the TBASE already available in ALCYONE allows advanced simulations of SAs from a precise description of the pre-accident state of the fuel. In this paper, after a brief presentation of ALCYONE, the burnup dependent Fission Gas Release (FGR) model developed for SAs is described. The evaluation of gradient related effects is then proposed from the simulation of the nominal irradiation of two fuel rods used in four VERCORS/VERDON tests (VERCORS 4 and 5, RT6 and VERDON 1). Comparison of global (pellet) and local (pellet rim or pellet center) FP releases with on-line measurements during these tests are used to assess the importance of the initial state of the fuel. Local differences in thermochemical equilibria are also discussed.

2 The fuel performance code ALCYONE

2.1 General description

ALCYONE is a fuel performance code co-developed by the CEA, EDF and FRAMATOME within the PLEIADES computational environment [26][28]. Multi-dimensional modeling (1.5D, 2D, 3D) of a fuel rod in normal and accidental conditions (Reactivity Initiated Accident [29], Loss of Coolant Accident [30]) is available in the code. In this work, only the 1.5D calculation scheme is considered. As illustrated in Figure 1, the fuel rod is discretized axially in slices and radially in annular rings.

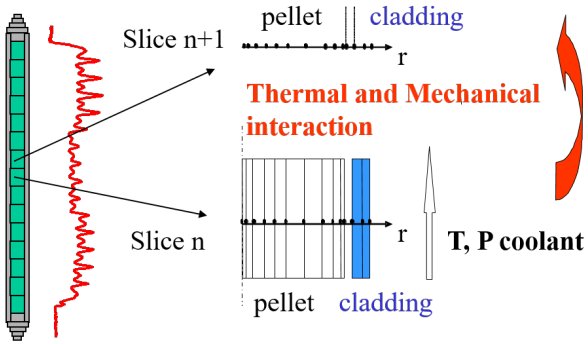

Figure 1: Typical fuel rod discretization in the 1.5D scheme of ALCYONE

A typical ALCYONE simulation of the fuel rod behavior during nominal irradiation relies on the 4 main following solvers:

- a thermo-mechanical solver to assess the stresses and the temperatures within the fuel pellet and the cladding rings,
- a neutronics solver to estimate the U and Pu fission-related power deposition within the fuel pellet rings as well as the local FP content,
- a fission gas solver to assess the Fission Gas Release (FGR) as well as the fuel swelling caused by FPs (including noble gases, i.e., Xe and Kr) within the fuel pellet rings,
- a thermochemical solver to estimate the compounds (composition and nature) formed by reaction between the FPs, actinides and oxygen within the fuel pellet rings.

The thermo-mechanical solver is based on the Finite Element (FE) code CAST3M [31] and provides the solution of the thermal heat balance equation and of the mechanical equilibrium equation for the fuel-clad system at hand with potential contact between the pellet and the cladding. Thermo-mechanical iterations are performed

until convergence is reached on a number of criteria related to temperature, stress, fuel-pellet gap and fuel swelling. More details can be found in reference [26].

The neutronics solver is called PRODHEL. The elements taken into account are: U, Pu, Am, Cm, Np, Xe, Kr, Cs, Rb, I, Br, Te, Se, Mo, Tc, Ru, Rh, Pd, Sr, Ba, Y, La, Nd, Pm, Eu, Gd, Ce, Pr, Nb and Zr. Overall, 199 isotopes of the FPs as well as 23 isotopes of the actinides are considered. The depletion and/or generation by radioactive decay of these isotopes is precisely assessed during the time spent by the fuel rod in the reactor. The database used for neutronic calculations is JEFF 3.1.1 [32]. This solver has been validated by cross-comparison with the reference neutronics codes APOLLO [33] and CESAR [34].

Two fission gas solvers are available in ALCYONE, named CARACAS [35] and MARGARET [36]. They provide a detailed description of the state of noble gases (Xe, Kr) in each fuel rings, whether dissolved in the fuel grains, in bubbles/pores in the grains or at the grain boundaries, or released in the free volume of the rod. Coupled calculations of fuel swelling related to bubble nucleation and growth are provided.

The OPENCALPHAD thermochemical solver ([37], [38]) has been implemented in ALCYONE [27] to provide in each fuel ring an estimation of the state (gaseous, solid, liquid) and composition of the compounds likely to form by chemical interactions between actinides, FPs and oxygen. The thermochemical database used with this solver is the TBASE detailed in Appendix A, initially developed for irradiation in nominal conditions. To reduce the chemical system, the FPs and actinides considered in the thermochemical calculations are grouped in 14 representatives elements [39]: inert fission gas (Xe for Xe+Kr+He), volatile FPs (I for I+Br, Te for Te+Se+Ag+As, Cs for Cs+Rb), stable oxides (Ba for Ba+Sr, Zr for Zr+Nb, Mo), metallic FPs (Ru for Ru+Tc+Rh, Pd for Pd+Sn+Sb), FPs and actinides in solid solution in UO_2 (Ce for Ce+Pr, Eu for Eu+Sm, La for La+Y, Gd for Gd+Nd+Pm, Pu for Pu+Np+Am+Cm).

As illustrated by the scheme of Figure 2, a simulation with ALCYONE includes several interactions between the solvers that rely on each other for the initialization of input variables.

Among the interactions of interest for this paper, it may be noticed that the initialization of thermochemical calculations (OPENCALPHAD) requires information from the neutronics solver PRODHEL (quantities of actinides and FPs) and from the thermomechanical solver CAST3M (temperature and mechanical pressure). OPENCALPHAD provides the composition of the chemical system at equilibrium in the fuel (gas phase, condensed phases, FPs dissolved in the uranium oxide matrix called solid solution in Figure 2). Evaluation of the FP release in each ring requires information (noble gas percolation flux) from the fission gas solver (MARGARET) and from thermochemistry (composition of the chemical system). Up to now, this scheme has been mostly used to study Pellet Cladding Interaction (PCI) failure of fuel rods during power ramps in experimental reactors [25][39][40] following irradiation in commercial reactors (base irradiation). In practice, ALCYONE simulations are therefore performed in two steps: first, the base irradiation of the fuel rod is assessed, second, the power ramp on part of the rod is simulated.

2.2 Extension to Severe Accident modeling

SA tests in experimental facilities such as VERCORS/VERDON are basically annealing tests at controled increasing temperature and atmosphere (oxidizing or reducing). The latter relies on the injection of a carrier gas of controled composition and at constant flow rate around the heated fuel rodlet. In practice, the modeling of SA tests in ALCYONE is straightforward and can follow a base irradiation simulation of the fuel rod (as done for a power ramp). The user can directly specify loading conditions in the input files such as the temperature history of the sample and the carrier gas composition history. The thermo-mechanical and neutronic solvers are used as is.

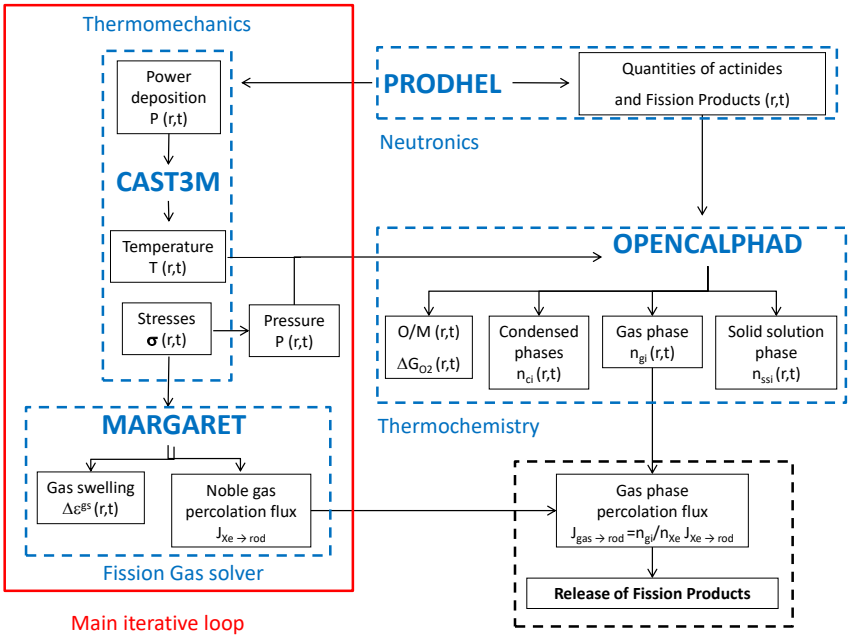

Figure 2: Schematic representation of the interactions in ALCYONE between the thermomechanical (CAST3M), neutronics (PRODHEL), Fission Gas (MARGARET), and thermochemical (OPENCALPHAD) solvers. (r, t) refer to the radial position of a ring and to a given time during the simulated irradiation sequence.

The thermodynamic database (called TBASE, originally developed for nominal irradiation conditions [39]) has been extended since the formation of new compounds from the reaction with the carrier gas (He, H_2O, H_2, O_2...) is expected during SA simulations. Validation of the thermochemical calculations on irradiated fuel with the updated TBASE and the OPENCALPHAD solver is based on cross-comparisons of results with similar calculations performed with the SGPS-SGTE database included in the FACTSAGE solver, as detailed in reference [41]. To improve the thermodynamic description of the Cs-Mo-Ba system in irradiated fuel, new compounds ($Cs_2Mo_2O_{7(s,l,g)}$ from experimental data recently published [42][43] and $ZrO_{2(ss)}$ from the TAF-ID [44] with s for solid, l for liquid, g for gas and ss for solid solution) have also been added, as detailed in reference [16].

The main difficulty is related to the modeling of Fission Gas Release (FGR) during SAs. As of today, the fission gas models available in ALCYONE (CARACAS and MARGARET) are not adapted to the conditions prevailing during SAs (uniform temperature in the fuel). In fact, they have been developed for normal irradiation conditions where the strong temperature gradient in the fuel pellet triggers FGR. Negligible FGRs are obtained in the case of a uniform temperature in the fuel. For this reason, a specific fission gas model has been implemented in ALCYONE for SAs. It describes the diffusion of all fission gases (noble gases and those formed from the chemical reactions between FPs) within an equivalent spherical fuel grain of radius a, according to the following equation:

$$\frac{\partial C}{\partial t} = \frac{1}{r^2}\frac{\partial}{\partial r}\left(Dr^2\frac{\partial C}{\partial r}\right) + \frac{\partial S_{FP}}{\partial t} \tag{1}$$

where C (mole/m^3) is the fission gas concentration, D (m^2/s) the effective diffusion coefficient and $0 \leq r \leq a$ (m) the radial position in the sphere. The novelty in this model resides in the term $\partial S_{FP}/\partial t$ added to take into account the gases formed by reaction between the FPs, as calculated by OPENCALPHAD. This term is essential to catch the release of semi-volatile FPs such at Ba that can take place after the total release of the volatile FPs. If it is not included in the diffusion equation, this may result in the total suppression of fission

gas release even if some FPs form gas compounds in the fuel. During an annealing test, as bubbles form inside the grains and as there is no resolution by fission spikes, most of the gases rapidly get trapped into the bubbles. So the gas transport within the grains is strongly believed to occur through intragranular bubble transport [45]. A single gas transport mechanism is thus believed to be sufficient to describe the release of both noble and chemically reactive FP gases together. The boundary condition is $C(r = a, t) = 0$ which is equivalent to an instantaneous release when gases reach the surface of the grain. The effective diffusion coefficient can be expressed as follows:

$$D(T) = D_0 \times \exp\left(-\frac{Q}{RT}\right) \tag{2}$$

where D_0 (m^2/s) is a constant parameter, Q (J/mol) the activation energy, R (J/(mol.K)) the universal gas constant and T (K) the temperature. In previous works on the VERCORS/VERDON tests [16][17], the fit of the measured release rate curves of ^{133}Xe has led to the following parameters: Q=188 kJ/mol, D_0=1.09×10^{-11} m^2/s for a fuel sample of average burnup 38 GWd/tU, D_0=2.17×10^{-10} m^2/s for a fuel sample of average burnup 72 GWd/tU. It must be emphasized that the impact of temperature, that present strong variations during the tests, was found to be reasonably well assessed with an activation energy of 188 kJ/mol (45 kcal/mol [46]), irrespective of the burnup. The impact of the burnup appears to be strong (factor 20 on D_0 when the burnup is approximately doubled) and cannot obviously be neglected in an ALCYONE simulation where a strong radial burnup gradient holds along the radius of the pellet. From a computational point of view, a simple and efficient way to account for the burnup dependency is to consider D_0 as a function of burnup. To determine the relation between D_0 and τ the burnup, it is best to use the well known approximate analytical solution of equation 1 (with $\partial S_{FP}/\partial t = 0$) giving the Fission Gas Release during an annealing test performed at a constant temperature T_0:

$$FGR = 6\sqrt{\frac{D'(T_0)t}{\pi}} \tag{3}$$

with $D'(T_0) = D(T_0)/a^2$ and t the time. Using the D_0 identified previously from the ^{133}Xe release rate curves of the VERCORS/VERDON tests (D_0=1.09×10^{-11} m^2/s at 38 GWd/tU and D_0=2.17×10^{-10} m^2/s at 72 GWd/tU), and assuming that the Fission Gas Release versus burnup relation can be described by a quadratic function (with FGR=0 at 0 GWd/tU), the following function for D_0 has been identified:

$$D_0(\tau) = 3.61 \times 10^{-9}\left(3.884 \times 10^{-5}\tau^2 + 3.435 \times 10^{-4}\tau\right)^2 \tag{4}$$

with τ the burnup in GWd/tU. To check the proposed function, it is of interest to compare the calculated FGRs to measurements made during the GASPARD test series [47] on standard irradiated fuels with average burnups between 48 and 72 GWd/tU. The tests were characterized by a slow or fast heating rate (0.2 to 20 °C) up to a temperature plateau of 1200 °C maintained during 15 minutes. Only the tests with a slow heating rate are considered here. All the samples were pre-irradiated in commercial reactors. The FGR versus burnup relation obtained from equations 3 and 4 is plotted in Figure 3 and compared to the measured FGRs. The 30 % FGR measured during a similar heating sequence performed on a 103 GWd/tU fuel sample [48] is also reported in the Figure. The graph also includes the FGR measured on a 96 GWd/tU large grain ($\sim$ 50 μm) fuel sample (17 %) that was pre-irradiated in a specific device in the Halden reactor ensuring a more uniform fission gas distribution by reducing the thermal gradients [49].

Considering the scattering of the measures, the proposed fission gas model gives a reasonable estimation of the burnup dependency of the FGR during the annealing tests considered. The proposed approach accounts for the burnup dependency of FGR during annealing tests by considering a burnup dependent diffusion coefficient. This is a convenient way of treating the problem in fuel performance codes but it may be argued that the physics behind this behavior is lacking. Several authors relate the increase of FGR with burnup to the increasing surface to volume ratio of the fuel accessible to fission gas in consequence of the evolution of the microstructure with irradiation [50][51][52] (cracking, interlinkage of fission gas bubbles at grain boundary, High Burnup Structure with decreasing grain size...). The proper implementation of these phenomena is out of the scope of the present

work since the purpose of the $D_0(\tau)$ relationship proposed here is to evaluate the impact of the burnup profile on FP release during SA, not to replace the sophisticated mechanistic models available in ALCYONE.

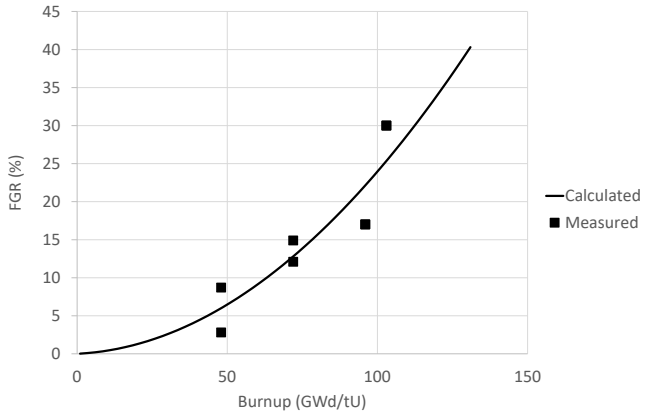

Figure 3: Calculated FGR versus burnup in annealing tests performed at $T_0 = 1200$ °C during $t = 15$ minutes and on UO_2 fuels with grain radius $a = 5$ μm, compared to measurements.

Meanwhile, it may be interesting to compare the present approach to the surface to volume ratio (S/V) evolution with burnup reported by Turnbull et al. [50] from measurements performed on polycristalline uranium dioxide samples irradiated at 1400 °C up to a maximum burnup of ~ 70 GWd/tU. The increase of the S/V ratio was reported to take place at a burnup of ~ 15 GWd/tU, marking the onset of open porosity in the fuel. Using the measured S/V at this burnup as a reference, it is possible to plot the relative increase of the S/V ratio as a function of burnup from the measurements of Turnbull et al. [50]. Since FGR in the burnup dependent model is a function of $D^{1/2}$, plotting the evolution of the relative increase of the S/V ratio as a function of burnup is equivalent to a plot of $(D(\tau)/D(\tau = 15))^{1/2}$ from the model. The comparison to the measurements is proposed in Figure 4.

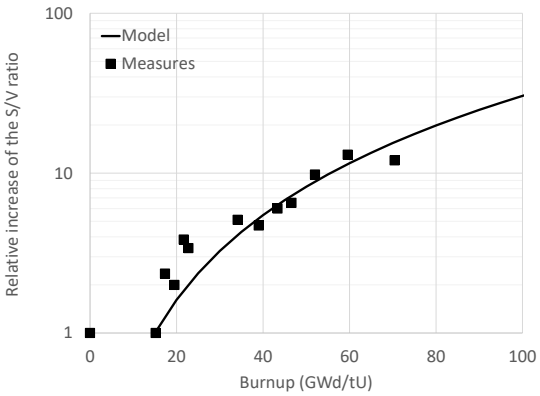

Figure 4: Relative increase of the S/V ratio versus burnup ($T_0 = 1400$ °C, $a = 5$ μm). Measured S/V ratios were extracted from Figure 3 of reference [50].

Figure 4 confirms that the proposed burnup dependent diffusion coefficient leads to a good estimation of the variation of the S/V ratio with irradiation. Similar trends for the evolution of the S/V ratio are reported by Amaya et al. [51] from irradiation experiments in the Halden Reactor Project.

During the simulation of the SA sequence, equation 1 is solved at each time step and each node by the finite volume method leading an estimation of the gas flux J (in mole/(m^2.s)) at the grain boundary:

$$J = -D \left. \frac{\partial C}{\partial r} \right|_{r=a} \tag{5}$$

The release rate RR (in mole/s) at each time step and each node of a FP indexed i is obtained from the following expression:

$$RR(FP_i) = \frac{\int_S J dS}{\int_V C dV} \times \int_V c_{FP_i} dV \tag{6}$$

where $\int_V c_{FP_i} dV$ (in mole) is the content of the i-th FP in the gas phase in the grain (from thermochemistry), $\int_V C dV$ is the total gas content in the grain (in mole), V the grain volume (in m^3) and S the surface of the grain (in m^2). Equation 6 considers an average thermochemical response in the grains. Grains could potentially also have minor radial variation of thermochemical effects due to varying FP concentrations across the grain resulting from FP diffusion or grain growth. These effects are expected to be minor.

Note that the effective diffusion coefficient does not depend on the fuel Oxygen/Metal (O/M) ratio, as it is the case in some severe accident codes [18]. This dependency stems from the decoupling of FP thermochemistry and fuel oxidation/reduction modeling in these codes. The thermodynamic equilibrium calculations performed with OPENCALPHAD and the TBASE include both phenomena [16] meaning that any calculated change in the fuel O/M can lead to an increased or reduced proportion of FPs in the gas phase. In our view, it is therefore not necessary to modify the gas diffusivity with fuel oxidation since fuel oxidation already changes the proportion of FPs in the gas phase and hence their potential release rates. This is a "natural" consequence of the coupled approach proposed in this work.

3 Modeling of the VERCORS/VERDON tests

3.1 Experimental conditions during the selected tests

The simulated VERCORS and VERDON tests are here briefly described. Four tests are considered to investigate the impact of fuel burnup on FP release. Two were performed on samples (3 pellets long) taken from the same fuel rod irradiated up to an average burnup of 38 GWd/tU [1] (VERCORS 4 and 5). The two others used similar samples (2 or 3 pellets long) taken from a fuel rod irradiated up to an average burnup of 72 GWd/tU (VERCORS RT6 [1] and VERDON 1 [5]).

The experimental sequence was very similar in the four tests. A first temperature plateau was performed at around 400 - 500 °C under an He flow. The temperature was then increased until reaching 1250 - 1300 °C (VERCORS 4 and 5) or 1500 °C (VERDON 1 and VERCORS RT6) under an oxidizing atmosphere (high H_2O flow rate). These conditions were maintained during 60 to 75 minutes depending on the test. This step aimed at fully oxidizing the cladding. After the oxidizing plateau, one or several temperature ramps were applied with one or more plateaus at intermediate levels. Two different conditions were used. During the VERCORS 4 and VERDON 1 tests, the carrier gas composition (H_2/He) ensured that reducing conditions hold in the furnace. During the VERCORS 5 and RT6 tests, the carrier gas consisted of water vapor (H_2O) with a small amount of hydrogen (H_2) in order to ensure oxidizing conditions in the furnace. A detailed description of the experimental conditions is given in Table 1.

Table 1: Temperatures, carrier gas compositions and flow rates during the VERCORS 4, 5, RT6 and VERDON 1 tests. The green background refers to an He atmosphere, the red background to an oxidizing atmosphere and the blue background to a reducing atmosphere.

Tests	**H_2O flow rate (g/min)**	**H_2 flow rate (g/min)**	**He flow rate (g/min)**	**Experimental sequence**	**Atmospheric condition**
VERCORS 4	0	0	0.03	Cold plateau at 500°C	**He**
	1.5	0.012	0	Ramp from 500°C to 1250°C + plateau at 1250°C (65 min)	**Oxidizing**
	0	0.012	0.48	Ramp from 1250°C to 2261°C + plateau at 2250°C (30 min)	**Reducing**
VERCORS 5	0	0	0.03	Cold plateau at 400°C	**He**
	1.5	0.027	0	Ramp from 400°C to 800°C + plateau at 800°C (30 min) + ramp from 800°C to 1000°C + plateau at 1000°C (30 min) + ramp from 1000°C to 1300°C + plateau at 1300°C (75 min)	**Oxidizing**
	1.5	0	0	Ramp from 1300°C to 2250°C + plateau at 2250°C (30 min)	**Oxidizing**
VERDON 1	0	0	0.24	Cold plateau at 400°C	**He**
	1.5	0.027	0	Ramp from 400°C to 1500°C + plateau at 1500°C (60 min)	**Oxidizing**
	0.018	0.0198	0.36	Ramp from 1500°C to 2400°C with plateaus (∼10min) every 100°C from 2000°C to 2400°C	**Reducing**
	0	0	0.36	Ramp from 2400°C to 2600°C + plateau at 2600°C (20 min)	**He**
RT6	0	0	0.48	Cold plateau at 400°C	**He**
	1.5	0.027	0	Ramp from 400°C to 1500°C + plateau at 1500°C (60 min)	**Oxidizing**
	1.5	0	0	Ramp from 1500°C to 2200°C with various slopes	**Oxidizing**

3.2 State of the fuel prior to the VERCORS/VERDON tests

Before simulating the VERCORS/VERDON tests, a calculation is made with ALCYONE of the base irradiation of the two father rods to determine the radial burnup profiles as well as the radial FP profiles in the pellets of the tested samples. To this end, the father rods are discretized axially in 30 slices and radially in 45 elements (40 in the pellet and 5 in the cladding thickness). As shown in Figure 5, the fuel pellet mesh is refined at the periphery to better describe the formation of the HBS and the burnup/FP peaked profiles.

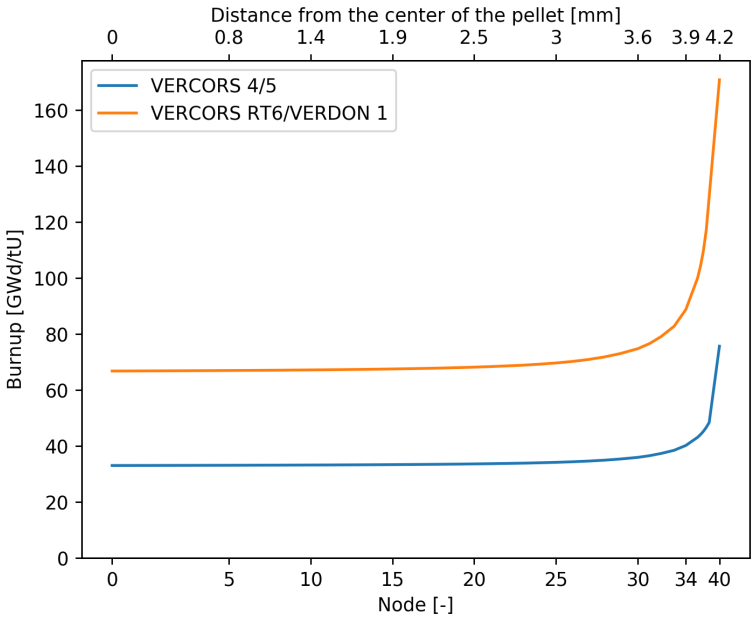

Figure 5: Calculated radial profiles of burnup in the fuel pellets used in the VERCORS 4/5 and RT6/VERDON 1 tests

The radial profiles of a number of FPs and actinides of interest calculated at the end of the base irradiation in the two fuel samples are plotted in Figure 6.

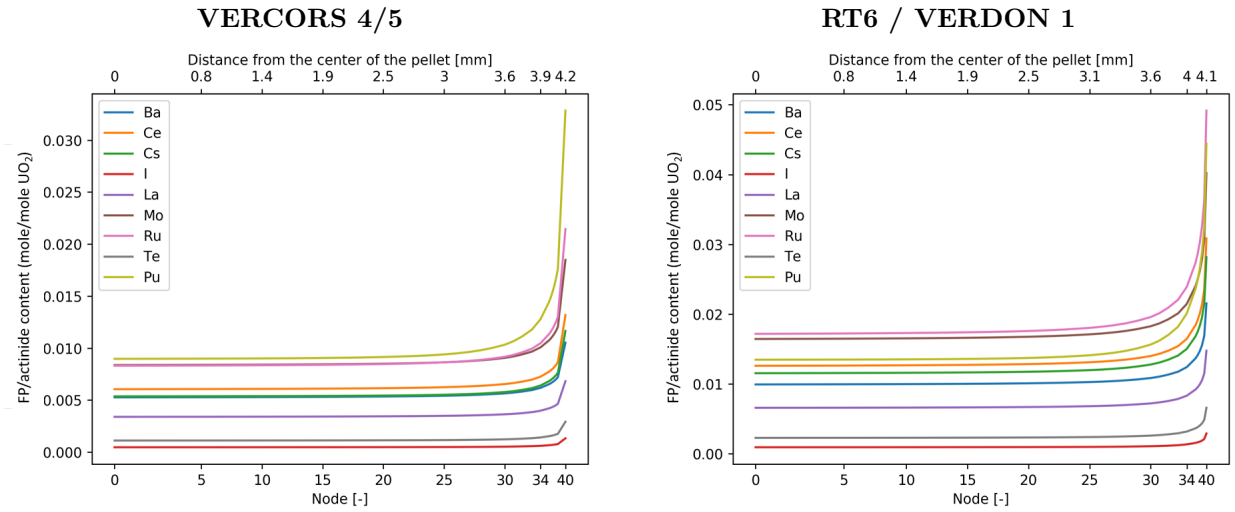

Figure 6: Calculated radial profiles of a selection of FPs and actinides (see section 2 for the complete list) in the fuel pellets used in the VERCORS 4/5 tests (left) and RT6/VERDON 1 tests (right)

The radial profile is nearly flat from the center to the last mm of the pellet. At the pellet rim, the burnup approximately doubles: from ∼35 GWd/tU till ∼70 GWd/tU in the medium burnup fuel of the VERCORS 4/5 tests and from ∼70 GWd/tU till ∼170 GWd/tU in the high burnup fuel of the RT6/VERDON 1 tests. The same trend is obtained for all the FPs with a doubling of their content at the pellet rim compared to the

pellet center. Among the actinides, Pu has a different behavior with a nearly threefold increase of its quantity at the pellet rim compared to the center. These burnup and FP radial gradients are used to initialize the thermochemical equilibrium calculations and the fission gas model in the simulations of SA tests that follow.

3.3 Modeling hypotheses during SA tests

In addition to the FP, actinide and oxygen contents of the fuel, the quantities of He, H and O from the carrier gas that enter the furnace at each time step are considered in the thermochemical equilibrium calculations since equilibrium between the fuel, cladding and the carrier gas is assumed to hold during the tests.

Another important hypothesis that was discussed in a previous paper [16] is that residual quantities of some gas compounds might remain in the furnace after they are removed from the carrier gas. This is of importance for the chemical speciation of FPs in the fuel which is highly dependent on the water or hydrogen content of the carrier gas even if it is very low. In the simulations presented in this paper, it is assumed that around 1% of the H_2O injected during the oxidation plateau of the VERCORS 4 and VERDON 1 tests (see the red boxes of Table 1) remains in the furnace during the high temperature part of these tests performed in reducing conditions (see the blue boxes of Table 1) .

While most of the FPs are located in the fuel pellets, potential reactions with the cladding are likely when they are released, as shown by post-test observations [3]. To account for that, part of the cladding Zr is included in the thermochemical calculations. In a previous work [16], it was shown that best-estimates of Ba release were obtained if 2% of the cladding Zr was considered in the thermochemical calculations of the VERCORS 4 test (reducing conditions at high temperature) and 10% in the VERCORS 5 test (oxidizing conditions at high temperature). The same percentages of cladding Zr will be considered here in the simulations of the 4 tests, depending on the oxidizing or reducing conditions at hand: 2% of the cladding Zr in the VERCORS 4 and VERDON 1 test simulations, 10% in the VERCORS 5 and RT6 test simulations.

3.4 Simulation scheme for SAs in ALCYONE

A typical coupled thermomechanical - thermochemical simulation of a SA with ALCYONE includes the following calculations at each time step:

- a thermomechanical calculation of the fuel pellet - clad system equilibrium with CAST3M ;
- after convergence of thermomechanics, thermochemical equilibrium calculations with OPENCALPHAD are performed at each node of the fuel pellet mesh to estimate the phase distribution and chemical speciation of FPs, the FP solubility and change in fuel stoichiometry. The local burnup, FP and actinide inventories are used as inputs together with the carrier gases (He and/or H and/or O) that have entered the furnace during the time step (with a nodal distribution depending on the local fuel element volume);
- the diffusion equation 1 with the source term derived from the thermochemical equilibrium calculation results is then solved at each node of the fuel pellet mesh. It leads to an estimation of the gas phase release at each node;
- the gas phase release calculated at each node of the mesh is then used with the gas phase chemical speciation to estimate the release of each FPs at each node (local release given by equation 6) and at the pellet scale (global release);
- the FP inventory at each node of the mesh is then updated. The carrier gases that have not reacted with the fuel pellet (i.e., that are not bound with actinides or FPs) are assumed to leave the furnace.

OPENCALPHAD calculations performed at each node of the pellet mesh and at each time step provide therefore a very detailed spatial description of the chemical speciation of FPs in the fuel pellet. In the next section, plots of chemical species and of FP release are shown at two nodes only (pellet center and rim) since these results are sufficient to discuss the burnup dependency of thermochemistry and FP release.

4 Simulation results

4.1 Integral results on FP release

The calculated cumulated release of Xe during the four simulated tests are compared in Figure 7 to measurements.

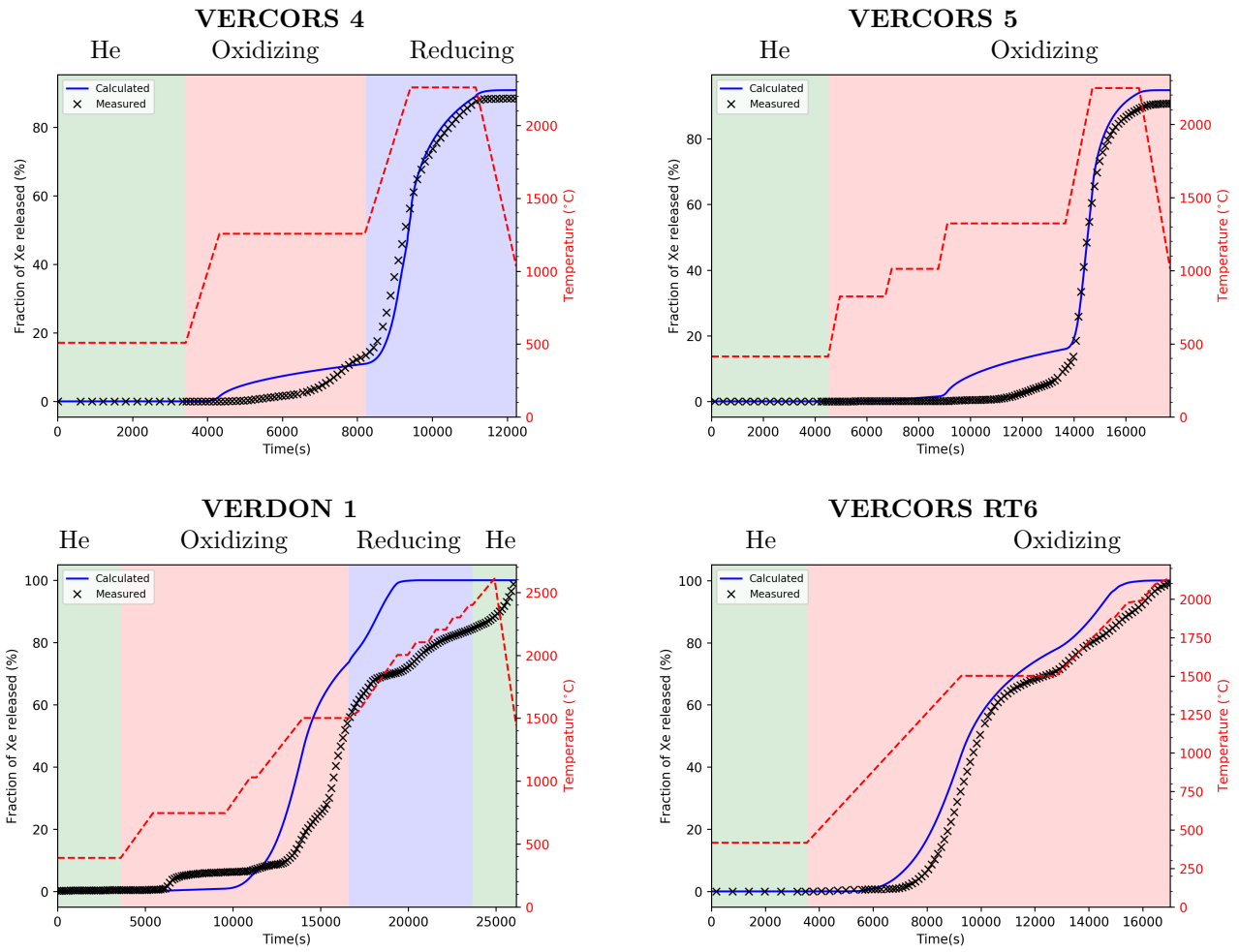

Figure 7: Measured and calculated cumulative release of Xe during the VERCORS 4/5 and RT6/VERDON 1 tests.

In most of the tests, the Xe release rate is well reproduced by the burnup dependent fission gas model. Only the VERDON 1 simulation presents significant differences with the measure, first during the oxidation plateau (the measured release takes place at the end of the plateau) and second during the following temperature ramps (slow release kinetics in spite of the high temperatures reached). It must be emphasized that the release of Xe is on the contrary well reproduced during the RT6 test that had a similar temperature history than the VERDON 1 test. In this respect, it is not possible to attribute the peculiar release kinetics during the VERDON 1 test to a burnup effect.

Figure 8 presents the calculated release of volatile FPs (iodine, tellurium and cesium) compared to measurements.

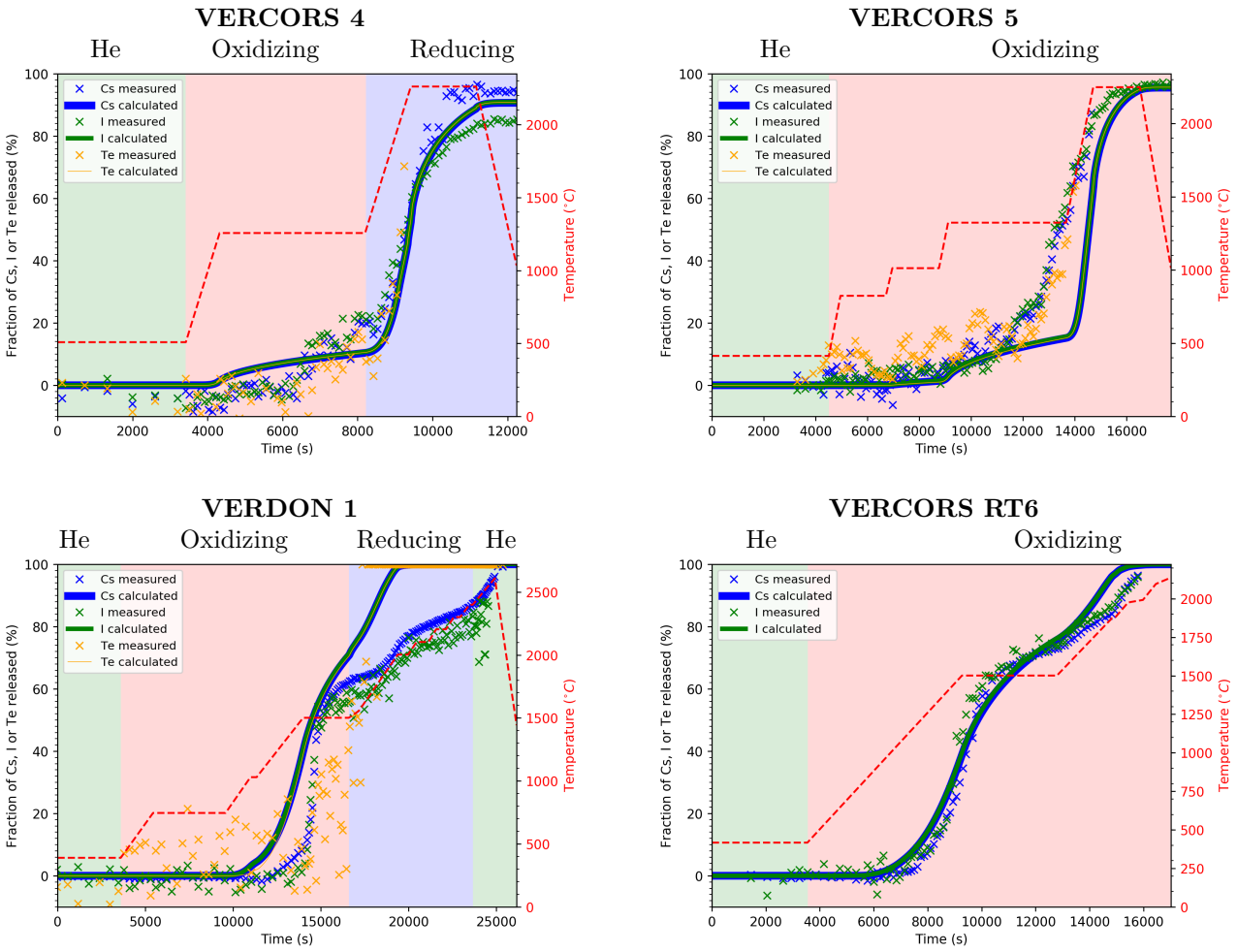

Figure 8: Measured and calculated fractions of iodine, cesium and tellurium released during the VERCORS 4/5 and RT6/VERDON 1 tests.

A very good agreement between calculations and measures is obtained for the volatile FPs during the VERCORS 4, 5 and RT6 tests. This result is a consequence of the quasi-total volatilization of the FPs at low temperatures and of the small impact of reducing/oxidizing conditions on their volatility. The release of iodine, cesium and tellurium is therefore mostly controled by the fission gas release model. In this respect, the poor agreement already observed for Xe during the VERDON 1 test is again visible for iodine, cesium and tellurium.

Figure 9 presents the calculated release of molybdenum and barium in the four simulated tests.

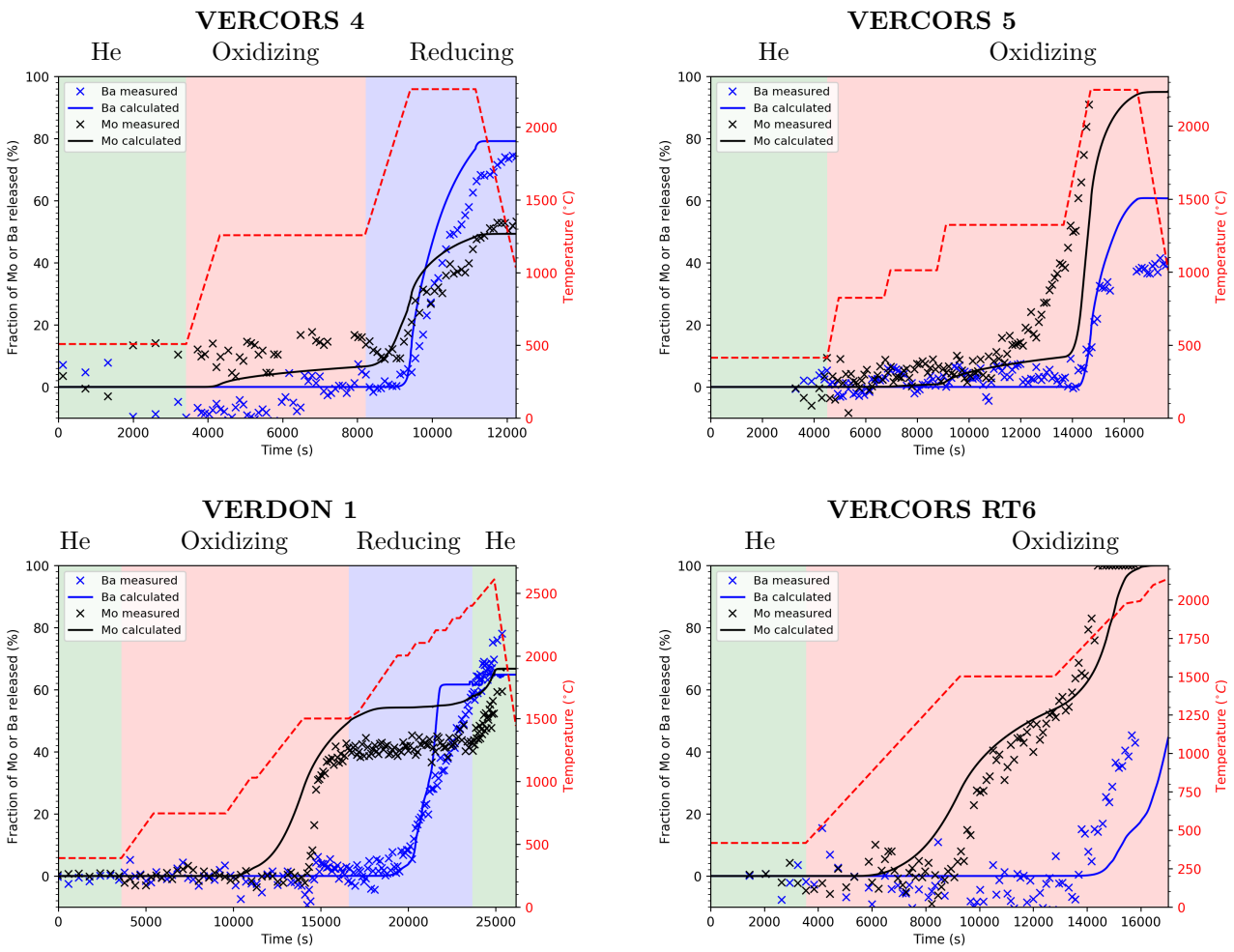

Figure 9: Measured and calculated fractions of barium and molybdenum released during the VERCORS 4/5 and RT6/VERDON 1 tests.

The release of the semi-volatile FP molybdenum is generally hard to assess due to the strong impact of thermochemistry on the availability of this FP in the gas phase [16], in particular in reducing conditions. Refinement of the TBASE by considering polymolybdates in the database ($Cs_2Mo_2O_7$) has improved the description of Mo release as it can be seen during the 1500 °C oxidizing plateau of the RT6/VERDON 1 tests (70% of the Mo inventory is found in $Cs_2Mo_2O_{7(g)}$ at the beginning of the temperature ramp to the oxidizing plateau). Since the fission gas model overestimates the release of Xe during the VERDON 1 test, the same trend is observed for Mo during the oxidizing plateau (55% calculated for 45% measured). The impact of oxidizing/reducing conditions after the oxidizing plateau is also well captured since the release of Mo is enhanced during the VERCORS 5 and RT6 tests compared to the VERCORS 4 and VERDON 1 tests. During the VERCORS 5 and RT6 tests, most of the remaining Mo is found in the gas phase in $Cs_2Mo_2O_{7(g)}$, $BaMoO_{4(g)}$, $MoO_{3(g)}$ and $Mo_2O_{6(g)}$. The Mo release rate limiting phenomenon is gas diffusion. During the VERDON 1 test, a stabilization of Mo release is observed after the oxidizing plateau in consequence of the reducing conditions at hand which lead to the precipitation of metallic Mo therefore suppressing Mo from the gas phase. The Mo release rate limiting phenomenon is thermochemistry.

Ba release is also strongly dependent on thermochemistry and therefore complicated to assess. In a previous work [16], it was determined that the barium partial pressure in equilibrium with the fuel and the cladding

depended on the quantity of Zr dissolved in the UO_2 solid solution as well as on the H_2O partial pressure. As explained previously, optimization of the calculated Ba release in the VERCORS 4/5 tests was achieved by considering 2%/10% of the clad Zr in the system in reducing/oxidizing conditions, respectively. As it appears from Figure 9, there is a general agreement between the calculated and measured Ba release curves in all the tests. The temperature at which release of Ba begins is well captured and is a consequence of the vaporization of barium molybdate and/or barium zirconate at around 1700°C. Differences with the measured release rates are observed in the VERDON 1 and RT6 tests that are related to the imperfect fission gas release model. In particular, the release of Ba seems to stop shortly after 20000 s in consequence of the 100% release of Xe, as shown in Figure 7.

4.2 Impact of the radial burnup profile on the FP release and the chemical speciation

Figure 10 compares the calculated fractions of Xe released at different radial positions in the pellet and for the whole pellet during the VERCORS 4/5 and RT6/VERDON 1 tests.

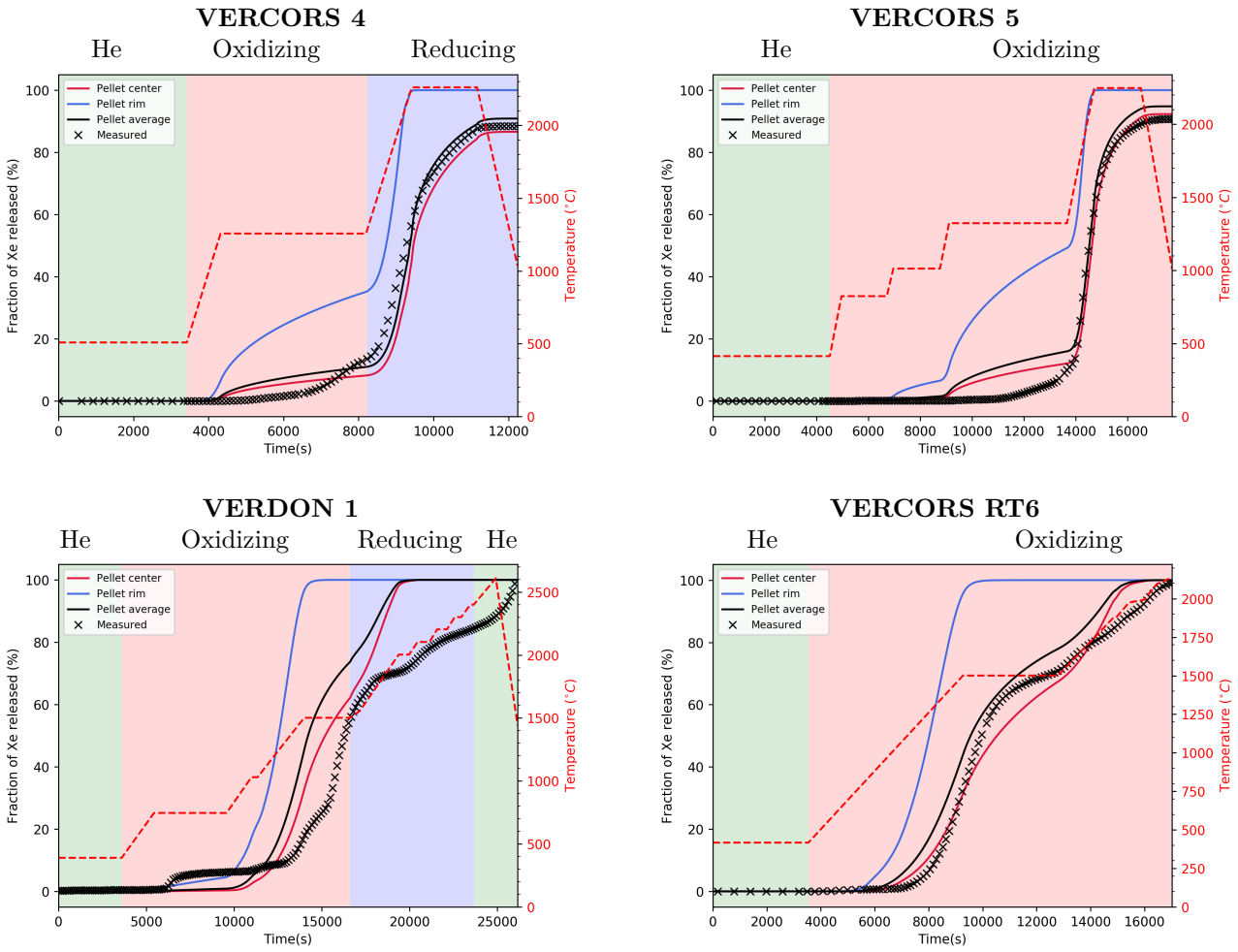

Figure 10: Calculated and measured fractions of Xe released at different radial positions in the pellet and for the whole pellet during the VERCORS 4/5 and RT6/VERDON 1 tests.

The impact of burnup on the fission gas release model is clearly seen in the graphs. The release of Xe at

the pellet rim, i.e., where the burnup is the highest, is systematically faster and greater in magnitude than at the pellet center. The impact on the pellet average release rate is however not very marked as shown by the comparison to the release rate at the pellet center. This result stems from the limited extension of the peaked radial burnup profile (approximately half a mm). The final releases from the whole pellet during the VERCORS 4/5 tests increase by around 5% in consequence of the burnup radial profile in the pellet. No impact is observed at the end of the RT6/VERDON 1 tests since the very high burnup at the pellet center ensures already a 100% release of Xe. The trend is the same for the volatile FPs iodine, cesium and tellurium, and is therefore not illustrated. Since measures of the residual Xe content along the pellet radius were not made during the VERCORS/VERDON programs, it is not possible to determine if these results are realistic.

The impact of the burnup radial profile on the release of the semi-volatile FP Mo is illustrated in the same way in Figure 11.

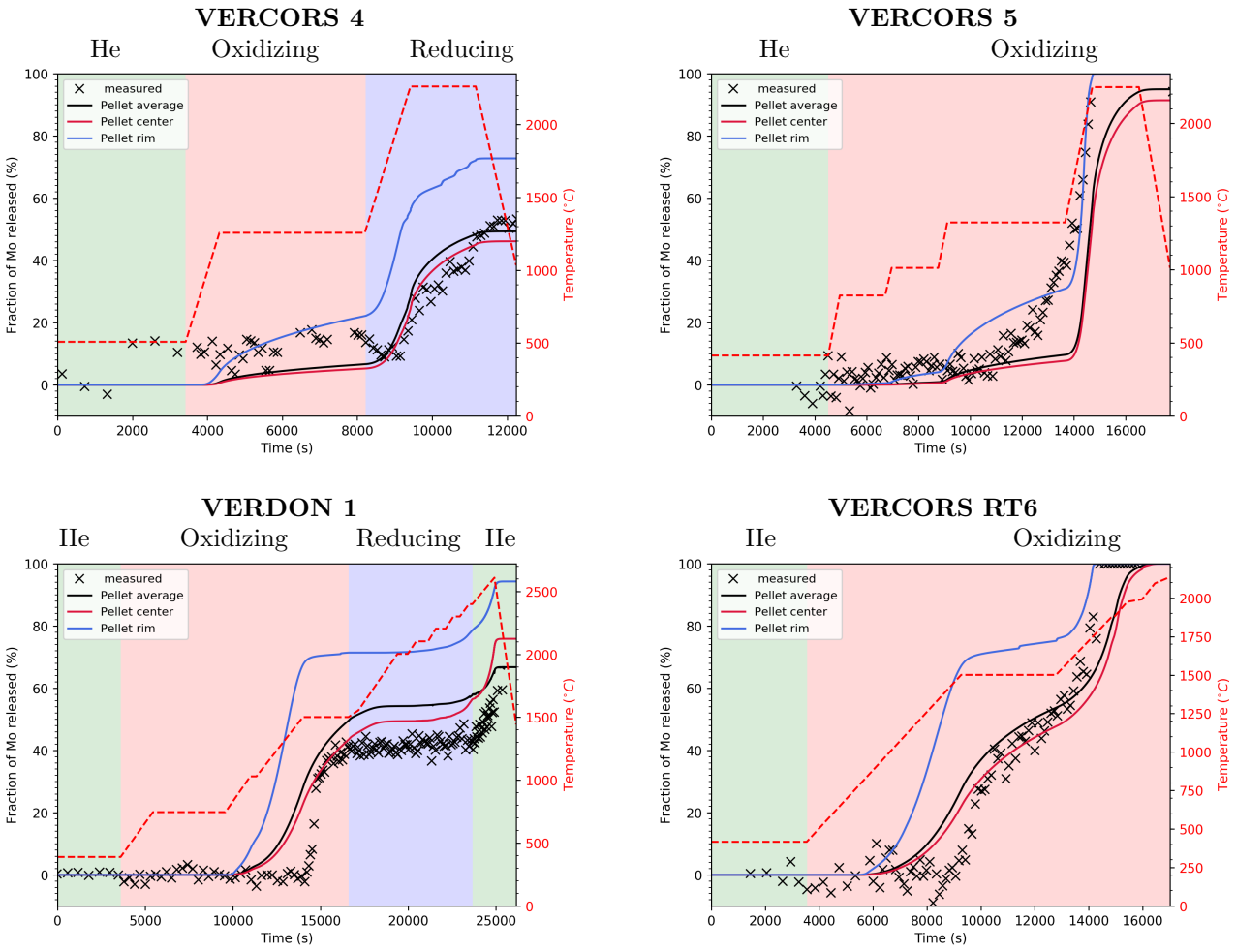

Figure 11: Calculated and measured fractions of Mo released at different radial positions in the pellet and for the whole pellet during the VERCORS 4/5 and RT6/VERDON 1 tests.

The calculated Mo release curves present the same features than those relative to Xe: the release rate at the pellet rim is systematically greater than at the pellet center; the release rate of the whole pellet is close to the release rate of the pellet center showing again the limited impact of the peaked burnup radial profile. Figure 12

gives the chemical speciation of Mo in the fuel during the RT6 and VERDON 1 tests at the pellet center and rim.

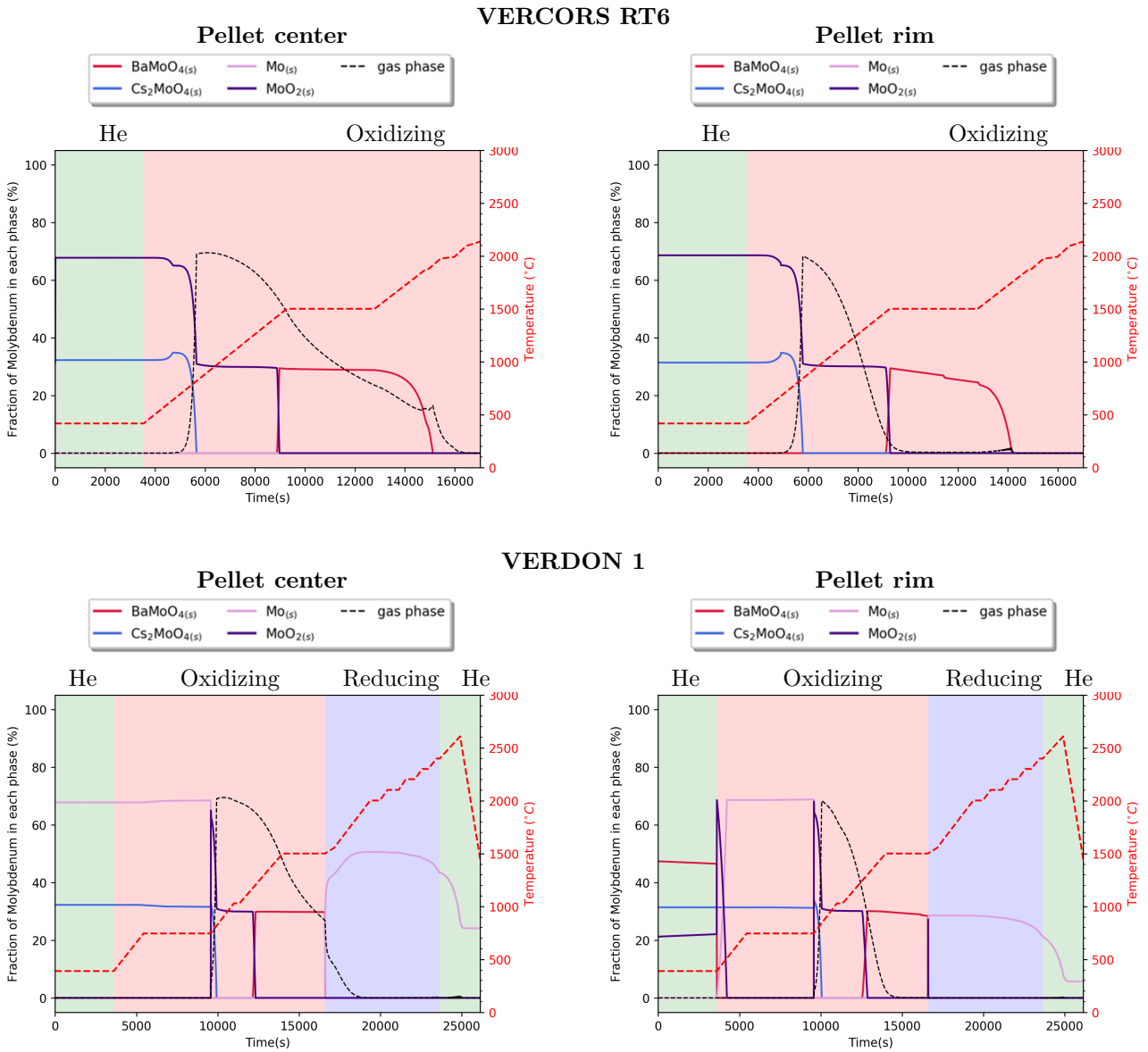

Figure 12: Calculated chemical speciation of Mo at the pellet center and rim during the RT6 and VERDON 1 tests

In spite of the differences in FP quantities between the fuel pellet center (70 GWd/tU) and rim (170 GWd/tU), the chemical speciation of Mo during the RT6 and VERDON 1 tests is not really dependent on the radial position in the pellet. During the RT6 test, 70% of the Mo becomes gaseous at ~800°C while the 30% remaining form $MoO_{2(s)}$. At ~1500°C, $MoO_{2(s)}$ dissociates and leads to the formation of $BaMoO_{4(s)}$. At the end of the oxidation plateau and during the following temperature ramp, the fast release of Mo from the fuel leads to the destabilization of $BaMoO_{4(s)}$ to provide additional Mo in the gas phase. As can be seen in Figure 12, the decrease of $BaMoO_{4(s)}$ at the pellet rim is faster than at the pellet center in consequence of the faster release of fission gases.

During the VERDON 1 test, the situation is similar till the end of the oxidation plateau where 30% of Mo is found in $BaMoO_{4(s)}$. The switch to a reducing atmosphere that follows leads to the precipitation of metallic $Mo_{(s)}$. A greater percentage of Mo in $Mo_{(s)}$ is found at the pellet center since Mo release at this radial position and during the oxidation plateau has been slower than at the pellet rim. The percentage of Mo remaining in the fuel is therefore more important at the pellet center. With the temperature increase that follows, conversion of $Mo_{(s)}$ into gaseous Mo occurs leading to a decrease of metallic Mo in the pellet and to an acceleration of Mo release, see Figure 11.

The chemical speciation of Ba during the RT6 and VERDON 1 tests at the pellet center and rim are shown in Figure 13.

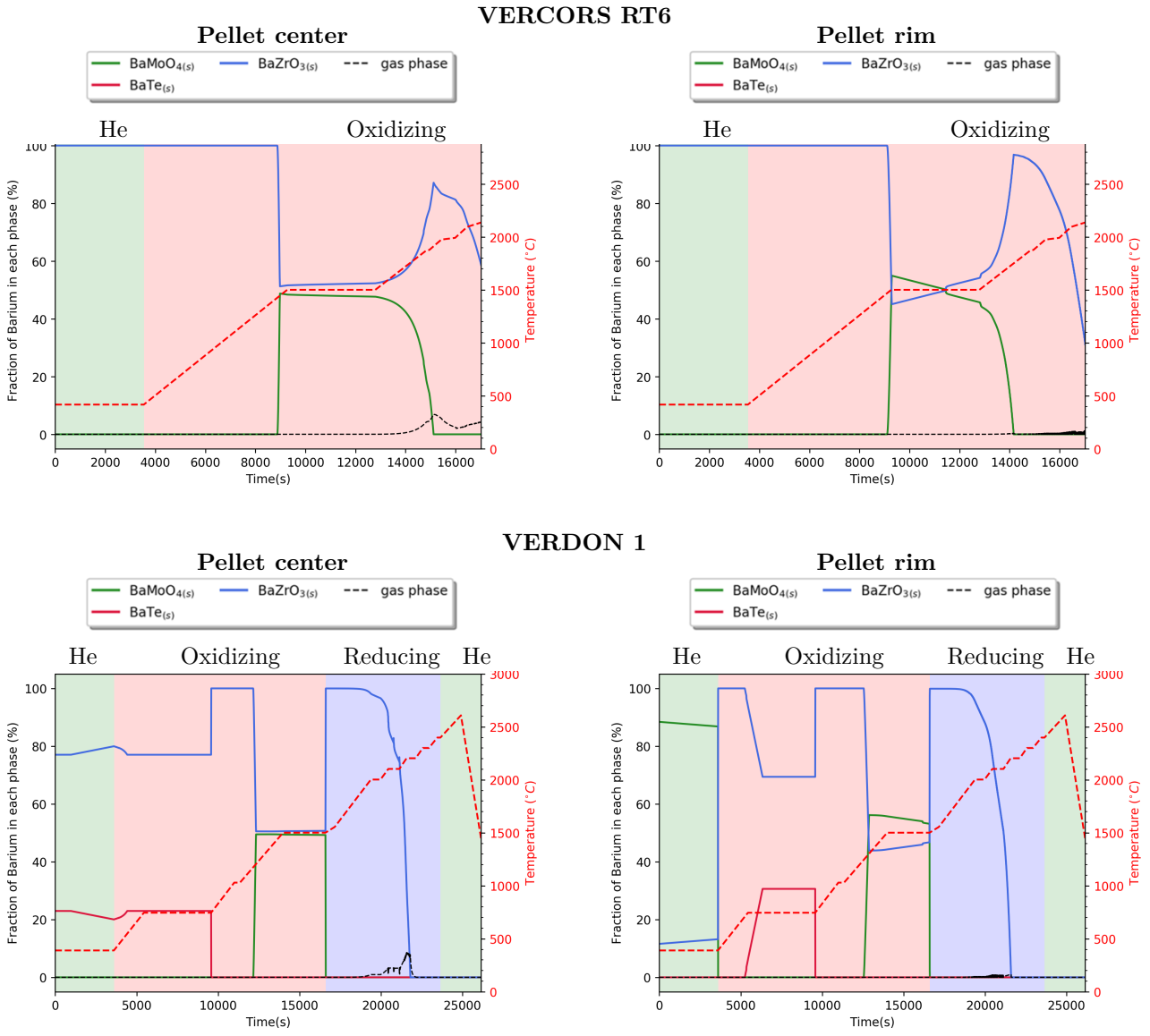

Figure 13: Calculated chemical speciation of Ba at the pellet center and rim during the RT6 and VERDON 1 tests

As can be seen, there is no great difference in the chemical speciation of Ba in the fuel pellet depending on

the radial position. During the oxidation plateaus of the RT6 and VERDON 1 tests, Ba is found approximately in the same quantity in $BaMoO_{4(s)}$ and $BaZrO_{3(s)}$. During the temperature ramp that follows in the RT6 test, conversion of $BaMoO_{4(s)}$ into $BaZrO_{3(s)}$ takes place till ∼1700°C where the progressive destabilization of $BaZrO_{3(s)}$ and the formation of gaseous Ba oxides or Ba molybdates explain the fast release of Ba, see Figure 9. The reducing conditions at hand during the high temperature ramp of the VERDON 1 test leads to the instantaneous conversion of $BaMoO_{4(s)}$ into $BaZrO_{3(s)}$ followed by its dissociation at ∼2000°C which explains the release of Ba from the fuel sample at this point. These graphs show that the chemical speciation of Mo and Ba is little modified by the radial burnup and FP profiles in the pellet. The most important factor for the release of semi-volatile FPs remains the burnup dependency of the FGR model.

5 Discussion

The simulations of the VERCORS and VERDON tests presented in this paper rely on a coupling between a fission gas release model and thermochemical calculations on the U-Pu-O-FPs system at hand in the fuel assumed in equilibrium with the carrier gas. The coupling has been integrated in the fuel performance code ALCYONE which is used to provide the state of the fuel before the SA tests and after the nominal irradiation in commercial reactors. By this way, the simulations can account for the radial burnup, actinides and FP profiles in the pellets and in particular for the peaks in burnup, Pu and FP content at the pellet rim. Samples with average burnups of 38 and 72 GWd/tU were considered in the SA simulations to investigate the impact of these peaks on the release of volatile and semi-volatile FPs. While a generally good agreement between calculated FP release rates and measurements was obtained, it was shown that the thermochemical equilibria (chemical speciation) in the fuel are fairly independent of the radial position in the pellet. The good agreement is thus a consequence of the three hypotheses introduced in a previous work where no radial profiles were considered [16]:

- the possible formation of $Cs_2Mo_2O_{7(s,l,g)}$ during the tests in consequence of their introduction in the thermodynamic database,
- the consideration of residual gases when the carrier gas composition is changed during the tests,
- the potential reaction of the fuel and FPs with part of the Zr cladding (2% in reducing conditions and 10% in oxidizing conditions).

The reasoning behind the introduction of $Cs_2Mo_2O_{7(s,l,g)}$ in the thermodynamic database has been discussed elsewhere [16][53] and will not be repeated here. The consideration of residual gases is based on measurements in a furnace with a precise control of the atmosphere [54]. The third hypothesis is consistent with the known reaction of the cladding with some FPs such as Te [3]. In the simulations, the Zr cladding is however introduced uniformely along the fuel pellet radius which is certainly far from reality. In practice and since a radial discretization of the pellet and of the cladding is used, fuel-clad-FP interactions should only take place at the pellet rim. Reactions between the oxidized cladding and the FPs released from the bulk of the fuel should also be introduced in some way in the simulations. This requires additional thermochemical calculations in ALCYONE that should be made at each node of the cladding and considering the FPs that are released from the fuel at each time step. Note that oxidation of part of the cladding (the 2 or 10% included in the fuel) is taken into account in the simulations. In the tests, all the Zr from the cladding is oxidized. This could be introduced in the simulations in the future by adding a mathematical description of oxygen diffusion in the cladding thickness [55]. Kinetics of Zr oxidation would by this mean be considered. This improvement of the model could also lead to a release of hydrogen that would then participate to the thermodynamic equilibrium of the fuel-clad-FPs system. As can be inferred, this could lead to a better estimation of Ba release that is at present slightly overestimated (Zr from the cladding triggers the formation of $BaZrO_{3(s)}$ and hence of gaseous Ba at temperatures above 1700°C).

The second point of improvement concerns the FGR model. The proposed approach depends only on burnup and does not take advantage of the precise assessment of fission gases provided by ALCYONE at the end of

base irradiation. Comparing the Xe release rate estimated with the burnup dependent FGR model during the VERDON 1 test with the measured Xe release rate in Figure 14, there is obviously room for improvement.

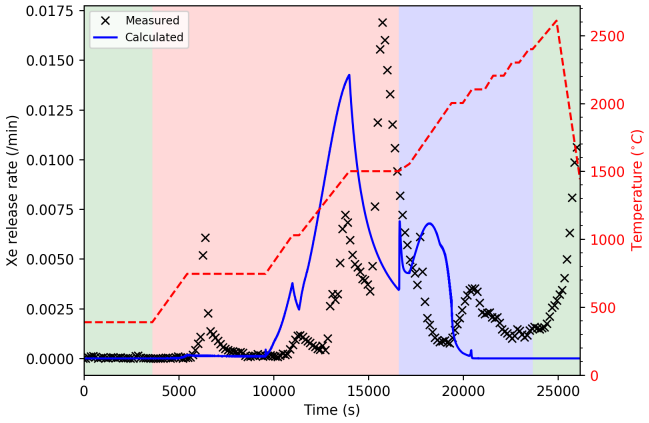

Figure 14: Calculated fission gas release rate during the VERDON 1 test compared to measurements.

The measured Xe release rate (black crosses in Figure 14) is characterized by five main peaks. The first one takes place during the first temperature plateau at 750°C, the second one starts at 1100°C during the following temperature rise to 1500°C, the main peak is seen during the 1500°C plateau, a fourth peak less significant starts at around 1800°C during the temperature ramp and a last puff occurs at the end of the temperature ramp. Obvously, the diffusion model developed in this work cannot describe such a complex behavior. Looking back at the cumulative Xe release plotted in Figure 7, the importance of each peak may be estimated: the first peak at 750°C represents 6% of the total Xe content of the pellet, the second one during the temperature ramp around 14%, the third one during the plateau at 1500°C represents around 50% of the total Xe content while the fourth and fifth peaks during the temperature ramp leads to an additional 20% and 10% release [5], respectively. The relationship between some of these peaks and the fission gas distribution in the fuel prior to an annealing sequence has been discussed by Pontillon et al. [56]. It was shown that the two peaks observed below 1200°C are related to the intergranular bubbles in the HBS region at the pellet periphery and to the intergranular precipitation zone found at the pellet center [57]. The release at higher temperatures (third and fourth peaks) is related to intragranular gas diffusion [5]. The fifth peak is attributed to the melting of the fuel and of the cladding that took place at 2650 °C [58].

ALCYONE simulations make use of the MARGARET model to describe the fission gas distribution in the fuel pellet during nominal irradiation. Precise information is obtained but has not been considered in the simulations of the SA sequences proposed in this paper. The evolution during base irradiation of the fission gas distribution calculated with MARGARET at several radial positions in the fuel pellet is illustrated in Figure 15.

The pellet center is submitted to high temperatures during nominal irradiation (∼1000°C) which explains the non negligible fission gas release calculated by MARGARET (around 10%). In consequence, the intergranular gas fraction that first increases till reaching 15%, decreases to 10% at the end of base irradiation. At mid-pellet radius, the lower temperature (700°C) explains the lack of fission gas release and the stable intergranular gas fraction at the end of in-reactor irradiation (around 12%). The behavior at the pellet rim is first similar with an increasing intergranular gas fraction that suddenly rises in consequence of the HBS formation to reach 35% at the end of the irradiation sequence. A progressive and steady FGR is calculated at the pellet rim during irradiation.

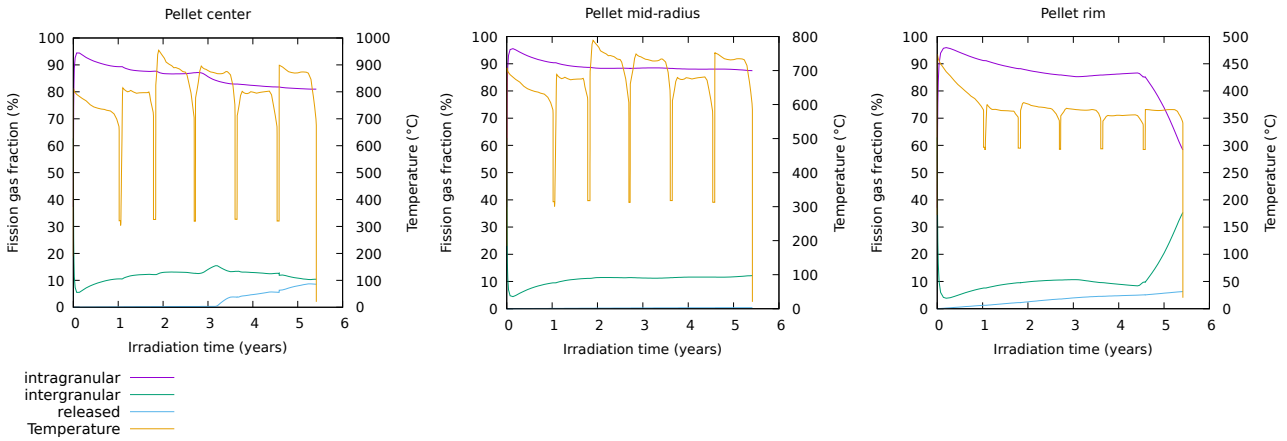

Figure 15: Calculated evolution of the fission gas distribution and temperature at the pellet center, mid-radius and rim during the base irradiation prior to the VERDON 1 test

Interestingly, the first peak is consistent with the calculated thickness of the HBS (0.5 mm) and the 30% intergranular gas fraction at the pellet rim that represent 6% of the total gas content in the fuel pellet. The calculated intergranular gas fraction outside of the pellet rim is close to 10-15%, which is more or less what is released from the pellet during the second peak. The third peak is therefore clearly related to the release of the bulk of the intragranular gas fraction. The fourth peak can be explained by the incomplete release of the intragranular gas fraction during the oxidation plateau of limited duration. This shows that the consideration of the fission gas distribution given by the MARGARET model could improve the modeling of FGR during the SA simulations. A differentiation of the FGR rates and of the temperature thresholds in function of the gas populations (intergranular in or outside the HBS, intragranular) should be considered if the multiple peaks measured during the SA tests are to be reproduced.

Conclusions

This work presents the first simulations of SA sequences with the fuel performance code ALCYONE. The coupling between irradiated fuel thermochemistry and fission gas release available in ALCYONE has been adapted to SAs by the refinement of the thermodynamic database, the consideration of the carrier gas in the thermodynamic equilibria and by the development of a specific burnup dependent FGR model. Simulations of 4 tests performed during the VERCORS and VERDON programs on fuel samples pre-irradiated in commercial reactors up to average burnups of 38 and 72 GWd/tU have been analyzed to investigate the impact of the radial burnup, FP and actinide profiles on the FP release rates. The precise assessment of the state of the fuel prior to the SA sequence is one of the advantage provided by the fuel performance code ALCYONE.

A reasonably good agreement between calculated and measured FP release rates during the four simulated tests was obtained with ALCYONE. The impact of oxidizing/reducing conditions on FP release rates was well reproduced in the case of the semi-volatile FPs Mo and Ba, showing the consistency of the thermodynamic modeling of the system. In spite of the strong evolution of the fission gas release rate with burnup considered in the model, the uneven radial distribution of burnup, actinides and FPs, was found to have little impact on the release of FPs from the pellets during the simulated SA sequences. The reasons behind this result are twofold. First, no marked difference in the chemical speciation of the volatile and semi-volatile FPs along the fuel pellet radius was obtained. Second, the radial extension of the region where the fuel burnup is significantly higher than at the pellet center is limited to the last half mm of the fuel pellet radius and therefore concerns a small volume of the pellet. These results fully justify the consideration of the whole pellet with average burnup, FP and actinide contents in SA codes.

The treatment of SAs in a fuel performance code originally dedicated to nominal irradiation simulations opens a wide range of potential sophistications of the models. First, the radial discretization of the fuel pellet and of the cladding provided in ALCYONE makes detailed calculations of the fuel rim - cladding interactions possible. Chemical reactions between the cladding and the FPs released from the fuel could also be described. The cladding progressive oxidation controled by the diffusion of oxygen in zirconia could easily be implemented. Finally, the proposed burnup dependent FGR model implemented in this work does not account for the precise evaluation of fission gas distribution within the fuel grains and grain boundaries that is provided by the MARGARET model in ALCYONE. It was shown that the intergranular fission gas fractions at the pellet center and in the HBS of the pellet rim are consistent with the magnitude of the low temperature Xe release rate peaks recorded during the VERDON 1 test. A refinement of the FGR model is therefore necessary to catch the complexity of the release mechanisms during SAs.

In the future, the coupled thermomechanics - thermochemistry scheme available in ALCYONE could help define doped fuels with specific FP retention capacities (Accident Tolerant Fuels) or design new VERDON tests. As of today, this work has been used to study the impact of new compounds [16] ($Cs_2Mo_2O_7$, dissolved ZrO_2 in the fuel) in the TBASE TDB on FP release during the VERCORS and VERDON tests.

Acknowledgements

The CEA authors would like to acknowledge EDF and FRAMATOME for their technical and financial support to this work.

References

[1] Y. Pontillon, G. Ducros, and P.P. Malgouyres. Behaviour of fission products under severe PWR accident conditions VERCORS experimental program — Part 1: General description of the programme. *Nuclear Engineering and Design*, 240(7):1843 – 1852, 2010.

[2] Y. Pontillon, G. Ducros, and P.P. Malgouyres. Behaviour of fission products under severe PWR accident conditions: The VERCORS experimental program — Part 2: Release and transport of fission gases and volatile fission products. *Nuclear Engineering and Design*, 240(7):1853 – 1866, 2010.

[3] Y. Pontillon, G. Ducros, and P.P. Malgouyres. Behaviour of fission products under severe PWR accident conditions. the VERCORS experimental program — Part 3: Release of low-volatile fission products and actinides. *Nuclear Engineering and Design*, 240(7):1867 – 1881, 2010.

[4] G. Ducros, P.P. Malgouyres, M. Kissane, D. Boulaud, and M. Durin. Fission product release under severe accidental conditions: general presentation of the program and synthesis of VERCORS 1–6 results. *Nuclear Engineering and Design*, 208(2):191 – 203, 2001.

[5] Y. Pontillon, E. Geiger, C. Le Gall, S. Bernard, A. Gallais-During, P.P. Malgouyres, E. Hanus, and G. Ducros. Fission products and nuclear fuel behaviour under severe accident conditions. Part 1: main lessons learnt from the first VERDON test. *Journal of Nuclear Materials*, 495:363 – 384, 2017.

[6] E. Geiger, C. Le Gall, A. Gallais-During, Y. Pontillon, J. Lamontagne, E. Hanus, and G. Ducros. Fission products and nuclear fuel behaviour under severe accident conditions. Part 2: Fuel behaviour in the VERDON-1 sample. *Journal of Nuclear Materials*, 495:49 – 57, 2017.

[7] C. Le Gall, E. Geiger, A. Gallais-During, Y. Pontillon, J. Lamontagne, E. Hanus, and G. Ducros. Fission products and nuclear fuel behaviour under severe accident conditions. Part 3: speciation of fission products in the VERDON-1 sample. *Journal of Nuclear Materials*, 495:291 – 298, 2017.

[8] M.H.A. Piro. Thermodynamically Informed Nuclear Fuel Codes—A Review and Perspectives. *Thermo*, 1(2):262–285, 2021.

[9] M.H.A. Piro. Thermodynamic predictions of CANDU fuel volatilization and fission product behaviour under severe accident conditions. *Journal of Nuclear Materials*, 558:153371, 2022.

[10] C. Guéneau, N. Dupin, L. Kjellqvist, E. Geiger, M. Kurata, S. Gossé, E. Corcoran, A. Quaini, R. Hania, A.L. Smith, et al. TAF-ID: an international thermodynamic database for nuclear fuels applications. *Calphad*, 72:102212, 2021.

[11] DH Barber. Implementation of a Gibbs energy minimizer in a fission-product release computer program. *Nuclear Review*, 2(1):39–48, 2014.

[12] R.O. Gauntt. MELCOR 1.8.5 Modeling aspect of fission product release, transport and deposition. Technical report, 1635, Sandia National laboratory, Albuquerque, USA, 2010.

[13] D.A. Kulik, T. Wagner, S.V. Dmytrieva, G. Kosakowski, F.F. Hingerl, K.V. Chudnenko, and U.R. Berner. GEM-Selektor geochemical modeling package: revised algorithm and GEMS3K numerical kernel for coupled simulation codes. *Computational Geosciences*, 17(1):1–24, 2013.

[14] Head-End Reprocessing studies by thermAl and thermoChemicaL treatment of fuElS. `https://www.psi.ch/fr/heracles/gems-specific-heracles-database`.

[15] S. Nichenko, J. Kalilainen, L.F. Moguel, and T. Lind. Modelling of fission products release in VERDON-1 experiment with cGEMS: Coupling of severe accident code MELCOR with GEMS thermodynamic modelling package. *Annals of Nuclear Energy*, 152:107972, 2021.

[16] A. Germain, J. Sercombe, C. Riglet-Martial, C. Introini, L. Noirot, Y. Pontillon, and P. Maugis. Coupled modeling of irradiated fuel thermochemistry and gas diffusion during severe accidents. *Journal of Nuclear Materials*, 560:153429, 2022.

[17] A. Germain, J. Sercombe, C. Riglet-Martial, C. Introini, L. Noirot, Y. Pontillon, P. Maugis, and C. Guéneau. Modeling of high burnup fuel thermochemistry, fission products release and fuel melting during the VERDON 1 and RT6 tests. *Journal of Nuclear Materials*, 561:153527, 2022.

[18] G. Brillant, C. Marchetto, and W. Plumecocq. Fission product release from nuclear fuel. I. Physical modelling in the ASTEC code. *Annals of Nuclear Energy*, 61:88 – 95, 2013.

[19] J. Noirot, L. Desgranges, and J. Lamontagne. Detailed characterisations of high burn-up structures in oxide fuels. *Journal of Nuclear Materials*, 372(2-3):318–339, 2008.

[20] J. Noirot, J. Lamontagne, N. Nakae, T. Kitagawa, Y. Kosaka, and T. Tverberg. Heterogeneous UO_2 fuel irradiated up to a high burn-up: Investigation of the HBS and of fission product releases. *Journal of nuclear materials*, 442(1-3):309–319, 2013.

[21] T. Barani, D. Pizzocri, F. Cappia, L. Luzzi, G. Pastore, and P. Van Uffelen. Modeling High Burnup Structure in oxide fuels for application to fuel performance codes. Part I: High Burnup Structure formation. *Journal of Nuclear Materials*, 539:152296, 2020.

[22] A. Magni, A. Del Nevo, L. Luzzi, D. Rozzia, M. Adorni, A. Schubert, and P. Van Uffelen. The TRANSURANUS fuel performance code. In *Nuclear Power Plant Design and Analysis Codes*, pages 161–205. Elsevier, 2021.

[23] M.S. Veshchunov, V.D. Ozrin, V.E. Shestak, V.I. Tarasov, R. Dubourg, and G. Nicaise. Development of the mechanistic code MFPR for modelling fission-product release from irradiated UO_2 fuel. *Nuclear Engineering and Design*, 236(2):179 – 200, 2006.

[24] T.R. Pavlov, F. Kremer, R. Dubourg, A. Schubert, and P. Van Uffelen. Towards a more detailed mesoscale fission product analysis in fuel performance codes: a coupling of the TRANSURANUS and MFPR-F codes. In *Topfuel conference*, Prague, Czech Republic, 2018.

[25] B. Baurens, J. Sercombe, C. Riglet-Martial, L. Desgranges, L. Trotignon, and P. Maugis. 3D thermo-chemical–mechanical simulation of power ramps with ALCYONE fuel code. *Journal of Nuclear Materials*, 452(1):578–594, 2014.

[26] J. Sercombe, B. Michel, and C. Riglet-Martial. 2.14 - Modelling of pellet cladding interaction. In R.J.M. Konings and R.E. Stoller, editors, *Comprehensive Nuclear Materials*. Elsevier, Oxford, 2020.

[27] C. Introïni, J. Sercombe, and B. Sundman. Development of a robust, accurate and efficient coupling between PLEIADES/ALCYONE 2.1 fuel performance code and the OpenCalphad thermo-chemical solver. *Nuclear Engineering and Design*, 369, 2020.

[28] B. Michel, C. Nonon, J. Sercombe, F. Michel, and V. Marelle. Simulation of Pellet-Cladding Interaction with the PLEIADES fuel performance software environment. *Nuclear Technology*, 182(2):124–137, 2013.

[29] J. Sercombe, T. Helfer, E. Federici, D. Leboulch, T. Le Jolu, A.H. De Ménibus, and C. Bernaudat. 2D simulation of hydride blister cracking during a RIA transient with the fuel code ALCYONE. *EPJ Nuclear Sciences & Technologies*, 2:22, 2016.

[30] A. Bouloré, C. Struzik, P. Goldbronn, I. Guenot-Delahaie, and J. Sercombe. Fuel behaviour modelling in accident conditions in ALCYONE fuel performance code. In *IAEA TECDOC 1913*, 2020.

[31] Cast3m. `http://www-cast3m.cea.fr`.

[32] JANIS 4.0 Java-based Nuclear Data Information System. `https://www.oecd-nea.org/janis/`.

[33] A. Santamarina, D. Bernard, P. Blaise, P. Leconte, R. Le Tellier, C. Vaglio-Gaudard, and J.-F. Vidal. APOLLO 2.8: a validated code package for PWR neutronics calculations. In *4th Topical Meeting on Advances in Nuclear Fuel Management*, volume 2, Hilton Head Island, South Carolina, USA, 2009.

[34] M. Vidal, R. Eschbach, A. Launay, C. Binet, and J.-F. Thro. CESAR 5.3: An industrial tool for nuclear fuel and waste characterization with associated qualification. In *Waste Management*, Phoenix, Arizona, USA, 2012.

[35] G. Jomard, C. Struzik, A. Boulore, P. Mailhé, V. Auret, and R. Largenton. CARACAS, an industrial model for the description of fission gas behavior in LWR-UO_2 fuel. In *WRFPM conference*, Sendai, Japan, 2014.

[36] L. Noirot. MARGARET: A comprehensive code for the description of fission gas behavior. *Nuclear Engineering and Design*, 241(6):2099 – 2118, 2011.

[37] B. Sundman, U.R. Kattner, M. Palumbo, and S.G. Fries. OpenCalphad - a free thermodynamic software. *Integrating Materials and Manufacturing Innovation*, 4(1):1, 2015.

[38] B. Sundman, U.R. Kattner, C. Sigli, M. Stratmann, R. Le Tellier, M. Palumbo, and S.G. Fries. The OpenCalphad thermodynamic software interface. *Computational Materials Science*, 125:188 – 196, 2016.

[39] P. Konarski, J. Sercombe, C. Riglet-Martial, L. Noirot, I. Zacharie-Aubrun, K. Hanifi, M. Frégonèse, and P. Chantrenne. 3D simulation of a power ramp including fuel thermochemistry and oxygen thermodiffusion. *Journal of Nuclear Materials*, 519:104–120, 2019.

[40] P. Konarski. *Thermo-chemical-mechanical modeling of nuclear fuel behavior. Impact of oxygen transport in the fuel on Pellet Cladding Interaction.* PhD thesis, INSA de Lyon, France, 2019.

[41] A. Germain, J. Sercombe, C. Riglet-Martial, Y. Pontillon, L. Noirot, C. Introini, and P. Maugis. Modeling of Fission Gas Release and irradiated fuel thermochemistry during severe accidents. In *Topfuel conference*, Seattle, Washington, USA, 2019.

[42] A.L. Smith, G. Kauric, L. van Eijck, K. Goubitz, G. Wallez, J.-C. Griveau, E. Colineau, Nicolas Clavier, and R.J.M. Konings. Structural and thermodynamic study of dicesium molybdate $Cs_2Mo_2O_7$: Implications for fast neutron reactors. *Journal of Solid State Chemistry*, 253:89–102, 2017.

[43] A.L. Smith, J. Vlieland, M.-C. Pignié, M. Abbink, G. Mikaelian, and P. Benigni. New insights into the Cs-Mo-O system: Experimental studies of the Cs_2MoO_4-MoO_3 pseudo-binary system. *Thermochimica Acta*, 696, 2021.

[44] C. Guéneau, N. Dupin, L. Kjellqvist, E. Geiger, M. Kurata, S. Gossé, E. Corcoran, A. Quaini, R. Hania, A.L. Smith, et al. TAF-ID: An international thermodynamic database for nuclear fuels applications. *Calphad*, 72, 2021.

[45] L. Verma. *Spatialized study of the coupling between extended defects and mobile species in the nuclear fuel.* PhD thesis, Aix-Marseille University, France, 2019.

[46] A.H. Booth. A method of calculating fission gas diffusion from UO_2 fuel and its application to the X-2-f loop test. Technical report, 496, Atomic Energy of Canada Limited, Chalk River, Canada, 1957.

[47] Y. Pontillon, M.P. Ferroud-Plattet, D. Parrat, S. Ravel, G. Ducros, C. Struzik, I. Aubrun, G. Eminet, J. Lamontagne, J. Noirot, et al. Experimental and theoretical investigation of fission gas release from UO_2 up to 70 GWd/t under simulated LOCA type conditions: the GASPARD program. In *International Meeting on LWR Fuel Performance*, Orlando, Florida, USA, 2004.

[48] J. Noirot, Y. Pontillon, S. Yagnik, J.A. Turnbull, and T. Tverberg. Fission gas release behaviour of a 103 GWd/tHM fuel disc during a 1200 °C annealing test. *Journal of Nuclear Materials*, 446(1-3):163–171, 2014.

[49] J. Noirot, Y. Pontillon, S. Yagnik, and J.A. Turnbull. Post-irradiation examinations and high-temperature tests on undoped large-grain UO_2 discs. *Journal of Nuclear Materials*, 462:77–84, 2015.

[50] J.A. Turnbull, C.A. Friskney, J.R. Findlay, F.A. Johnson, and A.J. Walter. The diffusion coefficients of gaseous and volatile species during the irradiation of uranium dioxide. *Journal of Nuclear Materials*, 107(2-3):168–184, 1982.

[51] M. Amaya, V. Grismanovs, and T. Tverberg. Changes of the surface-to-volume ratio and diffusion coefficient of fission gas in fuel pellets during irradiation. *Journal of Nuclear Materials*, 402(2-3):108–115, 2010.

[52] K. Une, K. Nogita, S. Kashibe, and M. Imamura. Microstructural change and its influence on fission gas release in high burnup UO_2 fuel. *Journal of Nuclear Materials*, 188:65–72, 1992.

[53] Ch. Riglet-Martial, J. Sercombe, and Y. Pontillon. Speciation and release kinetics of the fission products Mo, Cs, Ba and I from nuclear fuels in severe accident conditions. In *Topfuel conference*, Prague, Czech Republic, 2018.

[54] M. Khair. *Oxido reduction and speciation of corrosive fission products in oxide fuels: evaluation of the benefits of a p_{O_2} buffered fuel [In French].* PhD thesis, Bordeaux University, France, 2019.

[55] J.V. Cathcart, R.E. Pawel, R.A. McKee, R.E. Druschel, G.J. Yurek, J.J. Campbell, and S.H. Jury. Zirconium metal-water oxidation kinetics. IV. reaction rate studies. [BWR: PWR]. Technical report, 17, Oak Ridge National Lab., Tennessee, USA, 1977.

[56] Y. Pontillon, I. Moysan, S. Bernard, and M. Ledieu. New insight on volatile fission products (I and Cs) release from high burnup UO_2 fuel under LOCA type conditions. In *TopFuel conference*, Prague, Czech Republic, 2018.

[57] M. Marcet, Y. Pontillon, L. Desgranges, J. Noirot, J. Lamontagne, I. Aubrun, and B. Pasquet. High Burnup Structure Contribution to the Fission Gas Release under Transient Conditions. In *TopFuel conference*, Paris, France, 2009.

[58] E. Geiger, C. Guéneau, Y. Pontillon, and E.C. Corcoran. Modelling nuclear fuel behaviour with TAF-ID: Calculations on the VERDON-1 experiment, representative of a nuclear severe accident. *Journal of Nuclear Materials*, 522:294–310, 2019.

A Compounds considered in the TBASE for the thermochemical equilibrium calculations

The following phases and compounds are considered in the updated TBASE:

- The gas phase includes the following compounds: $Ba_{(g)}$, $Ba_{2(g)}$, $BaH_{(g)}$, $BaH_2O_{2(g)}$, $BaI_{(g)}$, $BaI_{2(g)}$, $BaMoO_{4(g)}$, $BaO_{(g)}$, $BaHO_{(g)}$, $Ba_2O_{(g)}$, $Ba_2O_{2(g)}$, $Ce_{(g)}$, $CeO_{(g)}$, $Cr_{(g)}$, $CrO_{(g)}$, $CrO_{2(g)}$, $CrO_{3(g)}$, $Cs_{(g)}$, $Cs_{2(g)}$, $CsI_{(g)}$, $Cs_2I_{2(g)}$, $Cs_2MoO_{4(g)}$, $Cs_2Mo_2O_{7(g)}$, $Cs_2O_{(g)}$, $Cs_2O_{2(g)}$, $CsO_{(g)}$, $CsHO_{(g)}$, $Eu_{(g)}$, $EuO_{(g)}$, $Eu_2O_{2(g)}$, $GdO_{(g)}$, $H_{(g)}$, $He_{(g)}$, $H_{2(g)}$, $HO_{(g)}$, $HO_{2(g)}$, $H_2O_{2(g)}$, $H_2O_{(g)}$, $HTe_{(g)}$, $HMo_{3(g)}$, $HMoO_{(g)}$, $HMoO_{2(g)}$, $H_2MoO_{2(g)}$, $H_2MoO_{3(g)}$, $H_2MoO_{4(g)}$, $I_{(g)}$, $I_{2(g)}$, $LaO_{(g)}$, $Mo_{(g)}$, $Mo_{2(g)}$, $MoI_{(g)}$, $MoI_{2(g)}$, $MoI_{3(g)}$, $MoI_{4(g)}$, $MoO_{(g)}$, $MoO_{2(g)}$, $MoO_{3(g)}$, $Mo_2O_{6(g)}$, $Mo_3O_{9(g)}$, $Mo_4O_{12(g)}$, $Mo_5O_{15(g)}$, $MoO_2I_{2(g)}$, $O_{(g)}$, $O_{2(g)}$, $O_{3(g)}$, $Pd_{(g)}$, $PdO_{(g)}$, $Pu_{(g)}$, $PuO_{(g)}$, $PuO_{2(g)}$, $Ru_{(g)}$, $RuO_{(g)}$, $RuO_{2(g)}$, $RuO_{3(g)}$, $RuO_{4(g)}$, $Te_{(g)}$, $Te_{2(g)}$, $Te_{3(g)}$, $Te_{4(g)}$, $Te_{5(g)}$, $Te_{6(g)}$, $Te_{7(g)}$, $TeI_{2(g)}$, $TeO_{(g)}$, $TeO_{2(g)}$, $Te_2O_{2(g)}$, $TeOI_{2(g)}$, $U_{(g)}$, $UO_{(g)}$, $UO_{2(g)}$, $UO_{3(g)}$, $U_2O_{2(g)}$, $U_2O_{3(g)}$, $U_2O_{4(g)}$, $U_2O_{5(g)}$, $U_2O_{6(g)}$, $Zr_{(g)}$, $ZrI_{(g)}$, $ZrI_{2(g)}$, $ZrI_{3(g)}$, $ZrI_{4(g)}$, $ZrO_{(g)}$, $ZrO_{2(g)}$.
- The liquid stoichiometric compounds included are: $Ba_{(l)}$, $BaH_2O_{2(l)}$, $BaI_{2(l)}$, $BaO_{(l)}$, $Ce_{(l)}$, $CeO_{2(l)}$, $Ce_2O_{3(l)}$, $Cr_{(l)}$, $CrO_{(l)}$, $Cs_{(l)}$, $CsHO_{(l)}$, $CsI_{(l)}$, $Cs_2MoO_{4(l)}$, $Cs_2Mo_2O_{7(l)}$, $Cs_2O_{(l)}$, $Cs_2O_{2(l)}$, $CsO_{2(l)}$, $Eu_{(l)}$, $EuO_{(l)}$, $Eu_2O_{3(l)}$, $Gd_{(l)}$, $Gd_2O_{3(l)}$, $H_2O_{(l)}$, $H_2O_{2(l)}$, $I_{2(l)}$, $La_{(l)}$, $Mo_{(l)}$, $MoO_{3(l)}$, $Pd_{(l)}$, $Pu_{(l)}$, $PuO_{2(l)}$, $Pu_2O_{3(l)}$, $Ru_{(l)}$, $RuO_{4(l)}$, $Te_{(l)}$, $TeO_{2(l)}$, $U_{(l)}$, $UO_{2(l)}$, $Zr_{(l)}$, $ZrI_{2(l)}$, $ZrI_{3(l)}$, $ZrI_{4(l)}$, $ZrO_{2(l)}$.
- The solid stoichiometric compounds included are: $Ba_{(s)}$, $BaH_2O_{2(s)}$, $BaI_{2(s)}$, $BaMoO_{4(s)}$, $BaO_{(s)}$, $BaTe_{(s)}$, $BaUO_{4(s)}$, $BaZrO_{3(s)}$, $Ce_{(s)}$, $Ce_2O_{3(s)}$, $Cr_{(s)}$, $Cr_2O_{3(s)}$, $Cs_{(s)}$, $CsHO_{(s)}$, $CsI_{(s)}$, $Cs_2MoO_{4(s)}$, $Cs_2Mo_2O_{7(s)}$, $Cs_2O_{(s)}$, $Cs_2O_{2(s)}$, $CsO_{2(s)}$, $Cs_2Te_{(s)}$, $Cs_2TeO_{3(s)}$, $Cs_2Te_4O_{9(s)}$, $Cs_2Te_4O_{12(s)}$, $Cs_2TeO_{4(s)}$, $Cs_2UO_{4(s)}$, $Cs_2U_4O_{12(s)}$, $Eu_{(s)}$, $Eu_2O_{3(s)}$, $Gd_{(s)}$, $Gd_2O_{3(s)}$, $I_{2(s)}$, $La_{(s)}$, $La_2O_{3(s)}$, $LaZr_2O_{7(s)}$, $MoI_{2(s)}$, $MoI_{3(s)}$, $MoI_{4(s)}$, $MoO_{2(s)}$, $MoO_{3(s)}$, $PdO_{(s)}$, $Pu_{(s)}$, $PuO_{(s)}$, $Pu_2O_{3(s)}$, $RuO_{2(s)}$, $RuTe_{2(s)}$, $Te_{(s)}$, $TeO_{2(s)}$, $U_{(s)}$, $UO_{3(s)}$, $U_3O_{8(s)}$, $U_4O_{9(s)}$, $U_3PuO_{8(s)}$, $Zr_{(s)}$, $ZrI_{2(s)}$, $ZrI_{3(s)}$, $ZrI_{4(s)}$, $ZrTe_{2(s)}$.
- The metal phase includes the following compounds: $Mo_{(s)}$, $Ru_{(s)}$, $Pd_{(s)}$.
- The solid solution phase includes the following compounds: $Ce_{3/4(ss)}$, $CeO_{2(ss)}$, $CrO_{3/2(ss)}$, $EuO_{(ss)}$, $Eu_{4/3}O_{2(ss)}$, $Gd_{4/3}O_{2(ss)}$, $La_{4/3}O_{2(ss)}$, $PuO_{2(ss)}$, $Pu_{4/3}O_{2(ss)}$, $U_{1/3(ss)}$, $UO_{2(ss)}$, $U_3O_{7(ss)}$, $UEuO_{3.83(ss)}$, $UGd_2O_{6(ss)}$, $ULa_2O_{6(ss)}$, $U_{1/3}Pu_{4/3}O_{2(ss)}$, $ZrO_{2(ss)}$.